Heat transfer performance and prediction of low global warming potential R134a refrigerant alternatives

by

Jordan Alexander Morrow

B.S., Kansas State University, 2016

AN ABSTRACT OF A DISSERTATION

submitted in partial fulfillment of the requirements for the degree

DOCTOR OF PHILOSOPHY

Alan Levin Department of Mechanical and Nuclear Engineering
Carl R. Ice College of Engineering

KANSAS STATE UNIVERSITY
Manhattan, Kansas

2022

Abstract

Due to the Kigali amendment, environmental regulations are phasing out high global warming potential (GWP) refrigerants such as R134a. Since many potential alternative refrigerants have flammability and cost concerns, minimizing system charge is critical. The condenser is typically responsible for 50% of the charge of a system; it is vital to have a fundamental understanding of the flow condensation heat transfer performance of low GWP refrigerants such as R513A and R450A. Flow condensation data were extracted from 35 papers and created a database of 5,030 condensation heat transfer coefficient data points. The data points were compared to predicted values from ten condensation correlations and the mean average error (MAE) for each one was calculated: Akers et al. (1959) (MAE=106%), Cavallini et al. (2006) (MAE=30%), Cavallini et al. (2011) (MAE=29%), Kim and Mudawar (2013) (MAE=28%), Macdonald and Garimella (2016) (MAE=61%), Shah (1979) (MAE=39%), Shah (2009) (MAE=32%), Shah (2013) (MAE=38%), Shah (2016) (MAE=26%), and Traviss et al. (1973) (MAE=46%). Many of the refrigerants in the database were not used for developing these correlations. Limited data were available for R513A (i.e., five studies) and R450A (i.e., one study). A vapor compression cycle experimental setup was designed and built to measure heat transfer performance of R134a alternative refrigerants. Experimental heat transfer coefficient data for R513A and R450A in a 0.95 mm diameter, multiport, mini-channel are presented for a range of mass flux (i.e., 200 – 500 kg/m^{2}s) and quality (i.e., 0.2 – 0.8) at a saturation temperature of 40°C. Condensation heat transfer coefficients for R134a, R513A, and R450A increased with increasing mass flux and quality. R513A condensation heat transfer coefficients were 2.6 – 25.6% lower than R134a heat transfer coefficients and pressure drop were 4.5 – 14.0% lower than R134a pressure drop. R450A heat transfer coefficients were 2.4% higher than R134a at high mass flux and quality

and up to 11.7% lower than R134a at lower mass fluxes than R134a heat transfer coefficients; R450A pressure drop were comparable to R134a pressure drop (i.e., 5.0% higher to 9.5% lower). A heat transfer coefficient correlation for low GWP (i.e., less than 750) refrigerants was developed using the Buckingham Pi theorem in conjunction with the MATLAB Optimization toolbox. The new correlation was developed using the condensation heat transfer coefficient database and the new experimental data collected from the experimental apparatus. The correlation is developed from a database of 4,110 data points including 11 synthetic refrigerants [i.e., R32, R41, R152a, R161, R450A, R452B, R454C, R455A, R513A, R1234yf, R1234ze(E)] and a range of diameters (i.e., 0.5 – 12.7 mm), saturation temperatures (i.e., 15 – 83°C), mass fluxes (i.e., 50 – 1200 kg/m^{2}s), qualities (i.e., 0.007 – 0.999), pressure ratios (i.e., 0.15 – 0.91), Bond numbers (i.e., 0.454 – 616), liquid Reynolds numbers (i.e., 347 – 80,084), liquid Prandtl numbers (i.e., 1.87 – 5.64), and vapor Weber numbers (i.e., 8.35 – 27,334). The correlation development used 80% of the data points and tested for accuracy with the other 20% of the data points. The new correlation has a MAE of 24.2% for the data used to build the correlation and a MAE of 24.6% for the data used to test the correlation. The consistency of the correlation to predict the build data points and the test data points shows that the correlation effectively predicts the condensation heat transfer coefficients of these low GWP refrigerants.

Heat transfer performance and prediction of low global warming potential R134a refrigerant alternatives

by

Jordan Alexander Morrow

B.S., Kansas State University, 2016

A DISSERTATION

submitted in partial fulfillment of the requirements for the degree

DOCTOR OF PHILOSOPHY

Alan Levin Department of Mechanical and Nuclear Engineering
Carl R. Ice College of Engineering

KANSAS STATE UNIVERSITY
Manhattan, Kansas

2022

Approved by:

Major Professor
Melanie M. Derby

Copyright

Abstract

Due to the Kigali amendment, environmental regulations are phasing out high global warming potential (GWP) refrigerants such as R134a. Since many potential alternative refrigerants have flammability and cost concerns, minimizing system charge is critical. The condenser is typically responsible for 50% of the charge of a system; it is vital to have a fundamental understanding of the flow condensation heat transfer performance of low GWP refrigerants such as R513A and R450A. Flow condensation data were extracted form 35 papers and created a database of 5,030 condensation heat transfer coefficient data points. The data points were compared to predicted values from ten condensation correlations and the mean average error (MAE) for each one was calculated: Akers et al. (1959) (MAE=106%), Cavallini et al. (2006) (MAE=30%), Cavallini et al. (2011) (MAE=29%), Kim and Mudawar (2013) (MAE=28%), Macdonald and Garimella (2016) (MAE=61%), Shah (1979) (MAE=39%), Shah (2009) (MAE=32%), Shah (2013) (MAE=38%), Shah (2016) (MAE=26%), and Traviss et al. (1973) (MAE=46%). Many of the refrigerants in the database were not used for developing these correlations. Limited data were available for R513A (i.e., five studies) and R450A (i.e., one study).

A vapor compression cycle experimental setup was designed and built to measure heat transfer performance of R134a alternative refrigerants. Experimental heat transfer coefficient data for R513A and R450A in a 0.95 mm diameter, multiport, mini-channel are presented for a range of mass flux (i.e., 200 – 500 kg/m^{2}s) and quality (i.e., 0.2 – 0.8) at a saturation temperature of 40°C. Condensation heat transfer coefficients for R134a, R513A, and R450A increased with increasing mass flux and quality. R513A condensation heat transfer coefficients were 2.6 – 25.6% lower than R134a heat transfer coefficients and pressure drop were 4.5 – 14.0% lower than R134a pressure drop. R450A heat transfer coefficients were 2.4% higher than R134a at high

mass flux and quality and up to 11.7% lower than R134a at lower mass fluxes than R134a heat transfer coefficients; R450A pressure drop were comparable to R134a pressure drop (i.e., 5.0% higher to 9.5% lower). A heat transfer coefficient correlation for low GWP (i.e., less than 750) refrigerants was developed using the Buckingham Pi theorem in conjunction with the MATLAB Optimization toolbox. The new correlation was developed using the condensation heat transfer coefficient database and the new experimental data collected from the experimental apparatus. The correlation is developed from a database of 4,110 data points including 11 synthetic refrigerants [i.e., R32, R41, R152a, R161, R450A, R452B, R454C, R455A, R513A, R1234yf, R1234ze(E)] and a range of diameters (i.e., 0.5 – 12.7 mm), saturation temperatures (i.e., 15 – 83°C), mass fluxes (i.e., 50 – 1200 kg/m^2s), qualities (i.e., 0.007 – 0.999), pressure ratios (i.e., 0.15 – 0.91), liquid Reynolds numbers (i.e., 347 – 80,084), liquid Prandtl numbers (i.e., 1.87 – 5.64), vapor Weber numbers (i.e., 8.35 – 27,334), and Bond numbers (i.e., 0.454 – 616). The correlation development used 80% of the data points and tested for accuracy with the other 20% of the data points. The new correlation has a MAE of 24.2% for the data used to build the correlation and a MAE of 24.6% for the data used to test the correlation. The consistency of the correlation to predict the build data points and the test data points shows that the correlation effectively predicts the condensation heat transfer coefficients of these low GWP refrigerants.

Table of Contents

List of Figures

List of Tables

Acknowledgements

I would like to thank Dr. Melanie Derby for being my advisor all these years. Your guidance and support through this journey of research and graduate school has been tremendous. You have helped me grow into the researcher I have become through guidance, support, patience, and I am sure a lot of frustration. I would like to thank my committee—Dr. Eckels, Dr. Fenton, and Dr. Hansen—for their feedback and guidance in different aspects of my research. I would like to thank the friends I have made in and out of the lab for the guidance, encouragement, support, and entertainment through all the ups and downs of graduate school. I want to thank Jarrod, Nhic, Brian, Carlos, and Josh, the wonderful undergraduate students who helped me build the apparatus, leak test, and run experiments. I would like to acknowledge the support from NSF grant #1828571.

I would like to thank my dad who was the one who suggested I be an engineer and started me on this journey. I only wish he could have been here to see it accomplished. I want to thank my mom who has always encouraged me to do my best and has supported me all these years. I would not have been able to do it without her. I want to thank my sister who has always had my back. I want to thank my giant family for all their support over the years. And, of course, I want to thank my wife Meg for her support as I chased my dream. I thank and praise God for the ability and perseverance He has given me.

Chapter 1 - Introduction

Refrigerants are measured on their environmental impact using two measures – ozone depletion potential (ODP) and global warming potential (GWP). ODP measures the negative impacts of a refrigerant released into the atmosphere on the ozone layer, while GWP is a value of how much more warming potential a refrigerant has than carbon dioxide (i.e., GWP=1). One molecule of a refrigerant with a global warming potential of 1000 produces an equivalent effect of 1000 molecules of carbon dioxide in the atmosphere. In 1987, the Montreal Protocol put into place a plan for phasing out refrigerants that had an ODP greater than zero (i.e., chlorofluorocarbons); these fluids were phased out and replaced with hydrofluorocarbons (HCFCs) and hydrofluorocarbons (HFCs), with most HCFCs being phased out later [1]. The F-Gas regulations in the European Union in 2015 and the Kigali Amendment to the Montreal Protocol in 2019 specified timelines for phasing out refrigerants that have a high GWP; these phase outs have now begun and will continue for years to come. Since the 2000s, a new category of refrigerants has been created called hydrofluoroolefins, or HFOs, which have GWPs less than 10. Other alternatives for high GWP refrigerants are natural refrigerants (e.g., propane and ammonia) and HFC/HFO mixtures. Natural refrigerants all boast extremely low GWP values (less than 10), while HFC/HFO mixture refrigerants have GWP values that generally range between 100 and 1000. This is still a drastic reduction in GWP compared to the incumbent HFCs, which have GWP ranges between 1000 to over 4000.

There are two factors that make this transition period to lower global warming potential refrigerants more difficult than the transition to zero ozone depletion potential. First, when phasing out refrigerants that had a non-zero ODP value, the line was very clear: the replacement refrigerants had to have ODP values of zero; however, the line for low GWP replacements is not

clearly set. Some regulations (i.e., F-gas regulations) do have a set value (i.e., GWP <150), but the majority do not. This makes it difficult to determine what reduction in global warming potential is sufficient. For example, a HFC/HFO mixture with a GWP of 500 could be replacing a HFC with a GWP of 4000, which is a 87.5% reduction in GWP, but some regulations could determine that this GWP value is too high. The other factor is that most alternative refrigerants have drawbacks. Natural refrigerants offer low GWPs but are often flammable, toxic, or both, or they run at very high pressures which increases costs. HFOs are mildly flammable, very costly, and show performance reductions. HFC/HFO mixtures have higher GWP values (compared to other alternatives) and some are mildly flammable; however, they tend to show less or no performance reductions compared to incumbent refrigerants. With phase outs beginning, research has been and is being done to figure out the best solutions. How do we keep the standard of human comfort while reducing the environmental impact of HVAC&R systems, while keeping people safe?

Attempts to mitigate the safety and cost drawbacks have designers reducing system component sizes to reduce the amount of refrigerant charge needed in the system. This is especially important in the condenser, which is typically the largest component of the refrigeration system [2]. Because of this, efficient design of these components is important to match the required performance with the smallest charge. One of the ways this is being accomplished, especially in condensers, is by moving to mini- and microchannel tubes; heat transfer performance increases with the decreasing diameter [3]. Because of this, characterizing condensation heat transfer performance of these alternative refrigerants is important. Some of these alternative refrigerants have been well characterized, but many of these alternative refrigerants are still greatly lacking data quantifying condensation heat transfer performance. Fundamentally understanding how these refrigerants perform is important for design and modeling, but it is also important to be able to

predict the performance of these refrigerants using correlations. There are several correlations that are widely used and accepted as being good predictors of heat transfer coefficients; however, most of these correlations were developed with few or no low GWP refrigerant alternatives. The need for good refrigerant heat transfer coefficient characterization in mini-channel tubes is critical for moving HVAC&R systems in a safe, efficient, and environmentally friendly direction.

Chapter 2 - Literature review

The chapter begins with an overview of R134a and its potential alternatives. Next, mini-channel condensation and flow regimes are discussed. Condensation studies of R134a, R513A, and R450A are discussed, and the chapter ends with a discussion of condensation heat transfer coefficient correlations.

2.1 R134a and its alternatives

R134a has been widely used since it was determined to be a promising alternative to R12 after the Montreal Protocol was signed by the United Nations in September of 1987 [4]. R134a is now one of the most widely used refrigerants on the market. It has been used in medium pressure applications including small refrigeration systems such as vending machines, mobile air-conditioning units, positive displacement and centrifugal chillers, domestic refrigerators, and small-scale medium temperature refrigeration systems [5].

New regulations including the Kigali Amendment to the Montreal Protocol and the F-Gas standard by the European Union are focused on phasing out refrigerants with high global warming potentials. Global warming potential (GWP) is a scale evaluating the refrigerant's global warming impact in the atmosphere compared to carbon dioxide (i.e., GWP=1). The global warming potential of R134a is 1300; R134a's GWP is substantially higher than the F-Gas standard (i.e, GWP=150) for domestic refrigerators and freezers and mobile air-conditioning units set by the European Union [5]. Therefore, research is being conducted on novel and existing refrigerants with potential for replacing R134a in new and existing HVAC systems. The major alternatives for R134a fall into four categories: natural refrigerants, low GWP HFCs, HFOs, and HFC/HFO mixtures. All four categories will be discussed with the HFC/HFO mixtures being the focus of this dissertation. Table 2.1 shows important information about R134a and some of its alternatives that will be

discussed in the following sections. Refrigerants are designated into safety groups depending on their toxicity and flammability. The safety group designation consists of a letter and a number; the letter designates the toxicity where A is lower toxicity class and B is higher toxicity class. The number designates the flammability where 1 is no flame propagation, 2 is low flammability, and 3 is high flammability. A new class (i.e., A2L) has been added for low flammability refrigerants that has a maximum burn velocity less than 10 cm/s.

Table 2.1 R134a and its alternative refrigerants

	R134a	R1234yf	R1234ze(E)	R513A	R450A	R600a	R152a	R516A
Group	HFC	HFO	HFO	HFO/HFC	HFO/HFC	HC	HFC	HFO/HFC
GWP	1300	1	1	573	547	3	138	131
Safety Group	A1	A2L	A2L	A1	A1	A3	A2	A2L

2.1.1 Natural refrigerants

Natural refrigerants are naturally occurring, or organic, compounds [e.g., ammonia (GWP=0), carbon dioxide (GWP=1)] and hydrocarbons [e.g., propane (GWP=3), isobutane (GWP=3)], some of which were part of the first generation of refrigerants [1]. Like many of the other refrigerants in the first generation, safety concerns shifted the focus to less volatile compounds (i.e., chlorofluorocarbons). However, some applications are dominated by these natural refrigerants. Isobutane and its blends are widely used in domestic refrigerators in Europe where the charge is small (i.e., less than a quarter of a pound), and industrial systems, especially food and drink processing, use ammonia, though its flammability and toxicity make it hard to appeal to other markets [1].

For replacing R134a, isobutane, propane, and their blends are promising alternatives. These hydrocarbons have very good thermodynamic and heat transfer properties [6], similar to or greater

than synthetic refrigerants [7]. The downside is their flammability; they are classified as ASHRAE A3 refrigerants. Hydrocarbons are currently widely used in domestic refrigerators, but the flammability makes it hard to use in larger systems for safety reasons [6]. Hydrocarbons have been shown to have higher heat transfer performance than synthetic refrigerants [7]. Reviews have shown that since hydrocarbon properties are closer to synthetic refrigerants, correlations typically do better at predicting performance [7, 8]. The reviews by Reddy et al. [9], Harby [10], and Babu [11] indicated that propane, isobutane, and their mixtures are good alternatives for R134a in small capacity domestic and commercial refrigerators. Harby [10] found through a synthesis of the literature that hydrocarbons and HC/HFC mixtures were the best alternatives showing 2.3 – 7.6% increase in COP, 4.4 – 18.7% reduction in energy consumed, and 40 – 56% reduction in refrigerant charge. Nawaz et al. [12] also notated that reducing the charge was beneficial to performance; reducing the charge also minimizes the flammability risk of these refrigerants. Babu [11] suggested that a 50/50% mixture of propane and isobutane was the best alternative for R134a in a domestic refrigerator. Dhavale and Deshmukh [13] found that propane/isobutane blends had a 35 – 40% reduction in charge and 5 – 10% reduction in energy consumption per day.

2.1.2 Low GWP hydrofluorocarbons (HFCs)

The other three alternative categories are considered synthetic refrigerants. Low GWP HFCs (i.e., R32, R152a) were considered when CFCs and HCFCs were being phased out, but more stable options (e.g., R134a) were selected due to their lack of flammability. These low GWP HFCs have GWP values between 100 and 1000. One low GWP is being considered as an R134a alternative – R152a. It has a low GWP (i.e., 138), but is a flammable refrigerant (i.e., A2). Several studies have found R152a to be more efficient than R134a [14-18]. Bellos and Tzivanidis [14] modeled a heat pump; the model predicted R152a had a 4.36% mean enhancement over R134a.

Bolaji [18] determined that R152a had 8.5% higher COP than R134a in a domestic refrigerator. Cabello et al. [15] experimentally determined that R152a had 13% higher COP than R134a, but had a decrease in cooling capacity. Sanchez et al. [17] presented R152a and R1234yf as the most promising R134a alternatives investigated. However, safety concerns surround the flammability of R152a; one option is in cascade systems, where studies have shown it to be a viable option [19-21].

2.1.3 Hydrofluoroolefins (HFOs)

Hydrofluoroolefins (HFOs) are a new class of refrigerants with very low GWP values (i.e., less than 10). They are more volatile than HFCs and therefore mildly flammable, classified as A2Ls, and therefore received a lot of attention for their very low GWP values, which are comparable to natural refrigerants. Most of the research done on HFOs is limited to two refrigerants – R1234yf and R1234ze(E). Both of these refrigerants are considered to be R134a alternatives, and there are limited HFO options suitable to replace other common HFCs, such as R410A or R404A [22]. Other HFOs that have received recent attention are R1234ze(Z), R1233zd(E), and R1243zf [23]. R1234ze(Z) is being considered as a replacement for R245fa [24-26], R1233zd(E) is being considered as a replacement for R123 [27] and R245fa [24, 26, 28, 29], R1243zf is being considered as a replacement for R134a [27, 30], and R1336mzz(Z) is being considered as a replacement for R245fa [28]. R1234ze(E) has shown comparable COP compared to R134a, but a reduced cooling capacity (up to 30%) requires modifications to account for the differences [31]. In condensation, R1234ze(E) has shown heat transfer coefficients 10% lower than R134a, and higher pressure drops than R134a [31]. R1234yf has shown to have similar or lower heat transfer coefficients than R134a [22], though one study found R1234yf to have higher heat transfer coefficients [32]. R1234yf has begun to be implemented in mobile air conditioning

units as a replacement for R134a [33]. In systems, R1234yf has shown similar cooling capacities to R134a with a slight reduction in COP [23]. One review said that R1234yf was a suitable drop-in replacement for R134a [23], while another suggested it not be a good drop-in due to R134a lubricant oil compatibility issues [33]. R1243zf has very limited data, but its properties suggest it would have similar performance to R134a [27].

2.1.4 Refrigerant mixtures

The fourth class of refrigerant alternatives are refrigerant mixtures. These mixtures typically contain a combination of HFCs, HFOs, and natural refrigerants, and they have GWP values on the order of 100 to 1000, are typically non-flammable or mildly flammable, and some have a temperature glide (i.e, at a constant pressure, the saturation temperature changes as the fluid moves from vapor to liquid due to the different saturation temperatures of the mixture components). Several refrigerant mixtures have been synthesized as alternatives to R134a – R430A [34-40], R436A [34, 35, 41-47], R440A [38, 48], R441A [48-52], R444A [35, 48, 53-56], R445A [34, 35, 48, 56], R450A [38, 53, 57, 58], R451A [48], R456A [34], R513A [53, 57-64], R513B [65], R515A [34, 53, 65], R515B [53, 65] and R516A [34, 53, 65]. Although all these refrigerants have received some attention in system performance studies, most of the research has focused on two alternatives R513A and R450A. Outside of R513A and R450A, fundamental condensation heat transfer studies are lacking.

R513A and R450A are two promising novel refrigerants that have GWP values less than half of R134a, but also do not introduce safety issues of flammable natural refrigerants and HFOs. R513A and R450A are medium pressure refrigerants with applications such as commercial and industrial refrigeration [5]. R513A is a mixture of R134a and R1234yf (44/56%) with a GWP of 631. R513A is a non-flammable (ASHRAE A1) refrigerant with no temperature glide (i.e.,

azeotropic). It has lower liquid thermal conductivity and lower vapor density than R134a. R450A is a mixture of R134a and R1234ze(E) (42/58%) with a GWP of 547. R450A is a non-flammable (ASHRAE A1) refrigerant with a temperature glide of 0.8 K at 40°C. R450A has higher vapor viscosity, and lower liquid and vapor densities than R134a.

2.2 R513A and R450A system performance

It is critical to understand the fundamental heat transfer performance of alternative refrigerants as well as their function in systems as potential drop-in replacements. Since the focus of this dissertation is fundamental condensation heat transfer, R513A and R450A system performance literature is briefly discussed, with the fundamental condensation heat transfer performance literature is discussed in subsequent sections.

2.2.1 R513A system performance

R513A has been investigated experimentally and theoretically as a potential drop-in replacement for R134a. Experimentally, R513A has been investigated in different systems including small scale vapor compression systems and mobile air conditioning units. Studies show that R513A typically has a modest reduction in COP (i.e., up to 9%) compared to R134a [57, 58, 66-72]; some studies have found R513A to have a higher COP [63, 73]. The studies by Yildiz and Yildirim [64] and Sjoholm and Ma [68] showed R513A to have higher COP than R134a at low evaporator temperatures (i.e., less than 0°C) and freezer conditions, suggesting its potential for use in freezer applications. R513A performed with a similar cooling capacity to R134a [57, 63, 66, 67, 69, 70, 73], though one study saw a 12% reduction in cooling capacity [71]. In theoretical studies, R513A performance modeled a 0 – 5% reduction in COP [74-76] and a small increase in cooling capacity [74]. R513A has also been investigated in drop-in applications looking to directly replacing R134a with R513A [77-79]. R513A was shown to be able to be used as a drop-in

replacement for R513A with minor modifications, such as a thermo-expansion valve adjustment [73]. R513A has also been investigated in the high temperature cycle of a CO_2 cascade system as a potential replacement and found to be a promising alternative [59, 80].

2.3.2 R450A system performance

R450A was investigated in different experimental and theoretical vapor compression systems. Experimentally, R450A has similar COP (up to 4% reduction) compared to R134a [57, 58, 66, 69, 81, 82]. The cooling capacity of R450A is considerably lower than R134a, however– somewhere between 6-23% depending on the study [57, 58, 66, 69, 81] due to the R1234ze(E) in R450A. Theoretical studies have seen R450A COP up to 7% higher and 3.4% lower than R134a [38, 74-76, 83-85]. Theoretical studies have also found R450A cooling capacity to be up to 10% lower than R134a [38, 75, 76, 83-85]. R450A was also found to be a potential drop-in replacement for R134a [79], including as a potential alternative for adsorption systems [86].

2.3 Overview of mini-channel condensation

Mini-channel tubes have garnered the interest of the HVAC industry to minimize refrigerant charge due to safety concerns of lower GWP refrigerant alternatives. The smaller diameter tubes can be used to minimize the refrigerant charge in systems where about 50% of the charge is found in the condenser [2]. While there is no universal criteria for distinguishing between macro- and mini-channels, the criteria by Kandlikar and Grande [87] is one of the more accepted criteria for mini-channels; the criteria states that macro-channels are greater than 3 mm, mini-channels are 0.2 – 3 mm [87, 88], and micro-channels are less than 0.2 mm. The rationale for the mini-channel criteria is based on manufacturing techniques. Channels below 3 mm are typically formed by narrow fin passages, and channels below 0.2 mm require a change in manufacturing techniques.

Along with the reduced refrigerant charge, another appeal of mini-channels is increased condensation heat transfer performance. Heat transfer coefficients have been found to increase with decreasing diameter [89, 90], though pressure drop increases as well. Condensation heat transfer coefficients also increased with increasing mass flux, with larger slopes at higher mass fluxes [90-92]. Heat transfer coefficients are also strongly dependent on quality, the mass fraction of vapor over the total mass of the liquid-vapor mixture, with increasing heat transfer coefficients with increasing quality [89-91]. However, Shin and Kim [90] and Matkovic et al. [93] found that quality had little to no effect on heat transfer coefficients at low mass flux (i.e., 100 – 200 kg/m^2s). This can be explained by the stratified flow regime (i.e., when the vapor phase flows on top of the liquid phase), in which heat transfer is temperature dependent and not affected by quality [91, 94]. Condensation heat transfer coefficients may increase with decreasing saturation temperature [89], although Derby et al. [92] showed saturation temperature had no significant impact. The decreasing temperature affects the thermophysical properties of the refrigerant affecting the heat transfer coefficient [95].

Channel shape can influence heat transfer coefficients. Shin and Kim [90] experimentally determined rectangular channels have higher heat transfer coefficients than circular channels at low mass flux, but circular channel heat transfer coefficients were higher at higher mass fluxes. Wang and Rose [96] modeled a rectangular channel which found that liquid pooled in the corners due to surface tension, which thinned the liquid film and lowered the heat transfer resistance. Agarwal and Garimella [97] investigated six different channel shapes; no conclusions could be draw about channel shape due to varying diameters. Derby et al. [92] investigated 1-mm diameter square, triangular, and semi-circular channels. Heat transfer coefficients were not found to vary with channel shape.

Understanding flow regimes and how they affect heat transfer performance is important for understanding and predicting heat transfer. Baker [98] developed a flow regime map using simultaneous oil and gas flows in 1, 2, and 4 inch pipes. Mandhane et al. [99] developed a liquid-gas flow regime map for horizontal flows in 0.5 – 6.5 inch pipes. Tandon et al. [100] developed a condensation flow regime map for horizontal flow. While these flow regime maps are well-known, Wang et al. [91] noted that they do not predict two phase refrigerant flow in mini-channels well. Coleman and Garimella [101] and Garimella [102] presented flow regime maps based on R134a experiments done in 1 – 5 mm diameter tubes for qualities between 0 and 1 and mass fluxes between 150 and 750 kg/m^2s. Four major flow regimes were presented: annular, wavy, intermittent, and dispersed. Liquid forms a ring around the wall with the vapor flowing within the ring in annular flow. Wavy flow is similar to annular in that the liquid forms a ring around the wall; however, in wavy flow, the liquid film is thicker at the bottom of the channel than the top, showing the effects of gravity on the flow. The differences in interfacial shear of the two phases cause waves to form at the liquid-vapor interface. Intermittent flow is similar to annular flow where the liquid forms an outer ring; however, in intermittent flow the vapor travels in periodic slugs or plugs that are broken up by liquid flowing between the slugs. Dispersed flow is when the liquid phase is turbulent and bubbles flow toward the top of the channel. As the velocities increase, the bubbles disperse throughout the channel [101, 102]. Cavallini et al. [103] described two condensation flow regimes – temperature dependent and temperature independent. Temperature dependent flow regimes are stratified flows where heat transfer is driven by temperature differences. These flows occur at lower mass fluxes and typically show little dependence on quality [91, 103]. Temperature dependent flows are annular or intermittent flows where heat transfer is dependent on convective forces. These flow regimes are greatly dependent on mass flux and

quality [91, 101-103]. As tube diameter decreases, the wavy (i.e., stratified) flow regime range shrinks as the influence of gravity decreases and the influence of surface tension increases [101, 102]. Because mini-channel condensation flow is typically dominated by annular flows, Coleman and Garimella [101] developed their flow map using mass flux and quality as the parameters. Nema et al. [104] used the R134a condensation flow regime data base covering 1 – 5 mm diameter tubes and mass flux of 150 – 750 kg/m^{2}s to develop non-dimensional transition criteria. Transition criteria for intermittent flow, discrete-to-disperse wavy flow, annular flow, and mist and dispersed flow are presented. The flow regime maps show good agreement with previous flow maps.

2.5 R134a condensation

R134a flow condensation heat transfer in mini-channels has been well studied and documented (Table 2.2). R134a condensation heat transfer coefficients increased with increasing mass flux and quality and decreased with increasing saturation temperature. Matkovic et al. [93] did observe that at low mass fluxes, heat transfer coefficients did not depend on quality. Bohdal et al. [105] investigated R134a and R404A in various diameters ranging from 0.31 mm to 3.30 mm. Macro-channel correlations (i.e., Dobson and Chato [106], Cavallini and Zecchin [107], Akers et al. [108], Shah [109], and Tang [110]) had limited ability to predict the performance of their data and proposed a new correlation. Kaew-On et al. [111] investigated R134a in 3.51 mm circular and flatted tubes. The flattened tubes produced heat transfer coefficients 5 – 400% higher than the circular tube depending on the aspect ratio. Sakamatapan et al. [112] investigated R134a in two multiport tubes and found that when the tube diameter reduced from 1.2 mm to 1.1 mm, the heat transfer coefficients increased 5 – 15%. Del Col et al. [113] compared the heat transfer performance of R134a based on channel shape and found heat transfer enhancement at the lowest mass flux, likely due to surface tension; no enhancement was found at higher mass fluxes. Del Col

et al. [114] investigated R134a in a single mini-channel in horizontal, vertical up flow, and vertical down flow. No differences in heat transfer coefficient were found in mass fluxes above 200 kg/m^{2}s; vertical down flow heat transfer coefficients were lower than the other two orientations as mass fluxes less than 200 kg/m^{2}s. Toninelli et al. [115] experimentally and numerically investigated multiple refrigerants in square and circular mini-channels; at low mass fluxes (i.e., less than 200 kg/m^{2}s), square channels showed heat transfer coefficient enhancement over circular channels due to the surface tension forces pulling liquid into the corners thinning the liquid film. Goss Jr. and Passos [116] investigated R134a in 0.77 mm diameter mini-channels and found heat transfer coefficients to be dependent on mass flux and quality. They also supported the idea that all the resistance to heat transfer in condensation is due to the conduction through the liquid film, especially at qualities less than 0.95. Rahman et al. [117] investigated R134a in multiport mini-channels with and without fins. Heat transfer coefficients increased with increasing mass flux and quality, and the heat transfer coefficients decreased with increasing saturation temperature due to the decreasing thermal conductivity in the liquid film with increasing saturation temperature. Yan and Lin [3] investigated R134a in a 2 mm diameter tube and compared their results to R134a results in a 8 mm diameter tube. They found R134a heat transfer coefficients to be 10% higher in the 2 mm diameter tube.

Table 2.2 R134a mini-channel condensation heat transfer studies (C-circular, R-rectangular, F-flattened, O-oval, SQ-square, S-smooth, MF-microfin, H-horizontal, VU-vertical up, VD-vertical down)

Author	Sat Temp (°C)	Mass Flux (kg/m^{2}s)	Diameter (mm)	Channel Characteristics
Bohdal et al. [105]	20-40	100-1300	0.31-3.30	C S H
Kaew-On et al. [111]	31-46	350-900	3.51 mm	C,F S H

Sakamatapan et al. [112]	35-45	340-680	1.1 mm (14), 1.2 mm (8);	R S H
Del Col et al. [113]	40	200-800	1.18 mm	SQ S H
Cavallini et al. 2006	40	278, 555	0.96 mm	C S H
Patel et al. [118]	35, 40	200-800	1 mm	C S H
Jige et al. [119]	40, 60	100-400	0.85 mm (17)	R S H
Del Col et al. [114]	40	100-790	1.23 mm	SQ S H,VU,VD
Toninelli et al. (2019)		65-200	C 0.96 mm, SQ 1.23 mm	C,SQ S H
Goss Jr. and Passos [116]	28-38	230-445	0.77 mm (8)	C S H
Rahman et al. [117]	30-35	50-200	0.64 mm (20), 0.81 mm (20)	R S,MF H
Wang et al. 2017	31.3	60-250	0.3016 mm (50	O S H
Yan and Lin [3]	25-50	100,200	2 mm (28	C S H
Matkovic et al. [93]	40	100-1200	0.96 mm	C S H
Wang et al. [91]	61.5-66	75-750	1.46mm (10)	R S H
Shin and Kim [90]	40	100-600	C 0.493, 0.691, 1.067mm; R 0.494, 0.658, 0.972mm	C,R S H
Garimella and Bandhauer 2001		150-750	0.76 mm	SQ S H
Coleman and Garimella [101]		150-750	C 4.91 mm; SQ 4 mm; R 4.8, 2.67 mm	C,SQ,R S H
Del Col 2010	40	200-1000	0.96 mm	C S H
Lopez-Belchi [61]	30-60	350-940	1.16 (10), 0.71 (19),	S,T S H
Li 2018	35, 40, 45	100-300	0.86 (15),	C S H
Park 2011	25-70	50-260	1.45 (7)	R S V
Del Col 2015	40	100-800	0.96mm,	C S H

Guo	35-45	200-400	2,	C S H
Morrow et al. [62]	36-40	300, 400, 500	0.72 (9),	R S H
Derby et al. [92]	35,45	75-450	1 mm (), square (7), triangular (5), semicircular (5)	S,T,semiC S H

2.6 R513A condensation

There is limited condensation heat transfer coefficient data for R513A. Much of the data were investigated in mini-channels (i.e., 0.72 – 2.5 mm) [61, 62, 95], while some were investigated in smaller macro-channels (i.e., 3.4 – 9.52 mm) [60, 120]. R513A heat transfer coefficients were investigated in smooth and microfin tubes, and in single channel [60, 95, 120] and multi-channel test sections [61, 62]. R513A increased with increasing quality and mass flux in five studies [60-62, 95, 120]. Higher mass fluxes present higher slopes because of the higher convective effect [95]. Morrow et al. [62] investigated R513A and R134a in 0.72 mm diameter multiport channels. R513A heat transfer coefficients were similar to R134a. Lopez-Belchi et al. [61] investigated R513A, R1234yf, and R134a in 1.16 mm diameter multiport channels. R513A heat transfer coefficients were about 10% lower than R134a, but R513A pressure drop was also about 10% lower. Diani et al. [60] investigated R513A in a 3.5 mm diameter smooth tube and 3.4 mm diameter microfin tube. The microfin tube showed greatest enhancement of heat transfer performance at lower mass fluxes (i.e., less than 400 kg/m^{2}s). Diani and Rossetto [95] investigated R513A in a 2.5 mm smooth tube and a 2.4 mm microfin tube and compared the data to R134a. R513A heat transfer coefficients were compared to R134a in the microfin tube and found to be about 10% lower than R134a, with greater differences at higher mass fluxes and qualities. R134a had higher performance due to its larger liquid thermal conductivity and lower vapor density. The lower vapor density means R134a has higher velocities at the same mass flux, meaning a greater convective

effect. R134a had about 10% higher pressure drop than R513A. In a larger diameter tube (i.e., 9.52 mm OD microfin), Karageorgis et al. [120] presented R513A heat transfer coefficients up to 10% greater than R134a at high mass flux and quality. The larger diameter tube and microfin configuration may have caused different flow regimes than in smaller diameters; however, the limited data makes any conclusions on conditions where R513A performs better than R134a. R513A also showed about 10% lower pressure drop than R134a. The majority of R513A were at a saturation temperature of 40°C [60-62, 95, 120], with a little data presented at 30°C [60, 95]. At a lower saturation temperature, the condensation heat transfer coefficients were higher because of the lower vapor density [95].

2.7 R450A condensation

Literature on R450A condensation heat transfer coefficients is very limited. Jacob et al. [121] conducted an experimental investigation in a 4.7-mm inner diameter smooth tube. The study investigated R450A at mass fluxes of 100 to 550 kg/m^{2}s, saturation temperatures of 45 and 55°C, and the full range of qualities. R450A heat transfer coefficients were found to increase with increasing mass flux and quality. R450A was compared to R134a and found to have lower heat transfer coefficients, but no more than 5% at higher qualities; however, R450A also showed an average of 8% higher pressure drop than R134a. In the other study, Liu et al. [122] presented simulation data of R450A using tube diameters of 1 and 2 mm. The simulations combined the SST k-omega model with the VOF model to explore condensation heat transfer coefficients. At mass fluxes of 400, 600, and 800 kg/m^{2}s, R134a showed 7.5-16.3% higher heat transfer coefficients than R450A. While limited, the simulated data suggest that the R1234ze(E) component of R450A does impact the condensation performance of R450A. With heat transfer coefficients up to 15%

lower than R134a and higher pressure drops than R134a, systems using R450A would need additional modifications to account for the performance degradations.

2.8 Condensation correlations

Correlations are important for predicting condensation heat transfer performance of refrigerants. Predictions are important for modeling and predicting performance of working fluids in design and research applications. Many correlations have been developed for macro-scale tubes [106, 108, 109, 123-128], but new refrigerants and the need for improved performance are leading to smaller diameter condensers. Some correlations—Wang et al. [91], Cavallini et al. [129], Cavallini et al. [94], Cavallini et al. [130], Bandhauer et al. [131], Shah [132], Kim and Mudawar [133], and Macdonald and Garimella [134]—have been developed for smaller diameter tubes, but few correlations in general have included new refrigerants. The ones that do are limited to one or two [e.g., R1234ze(E), R1234yf] [133, 134]. No correlation investigated included R513A or R450A in its development, though some correlations included its components [i.e., R134a, R1234yf, R1234ze(E)]. Correlations can be classified in two groups: correlations that require wall temperature [91, 94, 106, 119, 123, 127, 128, 131] and correlations that do not require wall temperature [108, 109, 124-126, 129, 130, 132-134]. Each type of correlation has its benefits, but wall temperature is not always known, especially in design situations.

A recent article by Morrow et al. [8] collected condensation heat transfer coefficient data from 35 low GWP synthetic refrigerant studies, encompassing 5,030 data points. Using the database, ten smooth tube correlations were investigated for their effectiveness for low GWP alternative refrigerants. The study focused on correlations that did not include wall temperature in their equations for two reasons – the database collected for the study did not include wall temperature for most of the data, and wall temperature is not always known when using

correlations. The correlations studied included Akers et al. [108], Cavallini et al. [130], Cavallini et al. [129], Kim and Mudawar [133], Macdonald and Garimella [134], Shah [109], Shah [124], Shah [125], Shah [132], and Traviss et al. [126]. Both R513A and R450A were included in the study. R450A was predicted under 20% MAE by several correlations. Cavallini et al. [130] was the best predictor, with Cavallini et al. [129], Kim and Mudawar [133], Macdonald and Garimella [134], and Shah [109] also predicting under 20% average MAE. It is important to note that there was limited R450A data (i.e., one study with 4.7-mm diameter tube). On the other hand, R513A was not predicted well by most of the correlations. Only two correlations (i.e., Shah [125] and Traviss et al. [126]) predicted R513A under a 50% average MAE. Limited data were available for R513A in the study as well (i.e., two studies with approximately 1-mm diameter tubes).

Three correlations were selected to compare to the new data collected in this dissertation – Kim and Mudawar [133], Shah [132], and Cavallini et al. [129]. Kim and Mudawar [133] was developed with 15 working fluids, including R1234yf and R1234ze(E). The correlation was developed with a diameter range of 0.424 – 6.22 mm and a mass flux range of 53 – 1403 kg/m^{2}s. The correlation used annular flow and non-annular flow as the basis for regime change using the modified Weber number and Lockhart-Martinelli parameter for calculating the transition criteria. The annular flow Nusselt number is calculated by

$$Nu_l = 0.048 {Re_l}^{0.69} {Pr_l}^{0.34} \frac{\varphi_v}{X_{tt}} \tag{2.1}$$

where Nu_l is the Nusselt number, Re_l is the liquid Reynolds number, Pr_l is the liquid Prandtl number, φ_v is the vapor two-phase multiplier, and X_{tt} is the turbulent-turbulent Lockhart-Martinelli parameter. The non-annular Nusselt number is calculated by

$$Nu_l = \left[\left(0.048 {Re_l}^{0.69} Pr_l^{0.34} \frac{\varphi_v}{X_{tt}} \right)^2 + \left(3.2 * 10^{-7} {Re_l}^{-0.38} {Su_{vo}}^{1.39} \right)^2 \right]^{0.5} \tag{2.2}$$

where Su_{vo} is the vapor-only Suratmann number.

The Cavallini et al. [129] correlation was developed using two working fluids, a diameter of 0.96 mm, and a mass flux range of 100 – 1200 kg/m^{2}s. The correlation was developed for low mass flux, with the annular flow model being used for mass fluxes greater than 200 kg/m^{2}s. The correlation heat transfer coefficient is

$$h = h_{LO}\left[1 + 1.128x^{0.8170}\left(\frac{\rho_l}{\rho_v}\right)^{0.3685}\left(\frac{\mu_l}{\mu_v}\right)^{0.2363}\left(1 - \frac{\mu_v}{\mu_l}\right)^{2.144} Pr_l{}^{-0.100}\right] \tag{2.3}$$

where

$$h_{lo} = 0.023 Re_{lo}{}^{0.8} Pr_l{}^{0.4}\frac{k_l}{D} \tag{2.4}$$

and x is quality, ρ_l is liquid density, ρ_v is vapor density, μ_l is liquid viscosity, μ_v is vapor viscosity, Pr_l is the liquid Prandtl number, and Re_{lo} is the liquid-only Reynolds number.

Shah [132] was developed as an improvement on the three previous versions with a specific focus on mini-channels. This version was developed with 13 working fluids, a diameter range of 0.1 – 2.8 mm, and a mass flux range of 20 – 1400 kg/m^{2}s. Like previous versions, this correlation has three regimes, using superficial velocity and vapor Weber number as transition criteria. The heat transfer coefficient for Regime 1 is

$$h_1 = h_{lo}\left[1 + 1.128x^{0.817}\left(\frac{\rho_l}{\rho_v}\right)^{0.3685}\left(\frac{\mu_l}{\mu_v}\right)^{0.2363}\left(1 - \frac{\mu_v}{\mu_l}\right)^{2.144} Pr_l{}^{-0.1}\right] \tag{2.5}$$

which is the same as Equation 2.3. The heat transfer coefficient for Regime 3 is

$$h_2 = 1.32 Re_l{}^{-1/3}\left[\frac{\rho_l(\rho_l - \rho_v)g k_l{}^3}{\mu_l{}^2}\right]^{1/3} \tag{2.6}$$

where h is the heat transfer coefficient, Re_l is the liquid Reynolds number, ρ_l is the liquid density, ρ_v is the vapor density, g is gravity, k_l is the liquid thermal conductivity, and μ_l is the liquid

viscosity. The heat transfer coefficient for Regime 2 is a combination of the heat transfer coefficients from the other two regimes.

2.9 Research objectives

As can be from the literature, both R513A and R450A have been shown to be promising alternatives to R134a, but limited data for both R513A and R450A make it difficult to draw any definitive conclusions on the effectiveness of either refrigerant or how they can be used in application. The limited heat transfer coefficient data makes predicting and modeling performance for design applications difficult. Therefore, the research objectives of this dissertation are to experimentally investigate the condensation heat transfer coefficients of R513A and R450A in a mini-channel condenser and compare them to R134a, investigate the capabilities of general correlations to predict these new low GWP refrigerants during flow condensation heat transfer, and present a new correlation developed from synthetic refrigerants with GWP values less than 750 that is capable of effectively predicting the new generation of synthetic and natural refrigerants.

Chapter 3 - Vapor compression cycle experimental apparatus

This chapter discusses the experimental apparatus used for data collection, the data reduction processes used, and the uncertainty calculations for the experimental data.

3.1 Vapor compression cycle

A vapor compression cycle experimental apparatus was designed and built to measure heat transfer coefficients for R134a and its alternatives (Figure 3.1). The refrigerant leaves the small compressor (Aspen 19-24-1101) as a high-pressure vapor that passes through a small oil separator (Temprite Model 320), pulling most of the compressor oil that escaped out of the refrigerant. The oil separator returns the oil back to the low-pressure side of the cycle by a capillary tube so that the oil returns to the compressor. Previous experiments using a Coriolis flow meter to measure refrigerant density showed less than 1% difference in expected refrigerant density, indicating that there is negligible oil circulating through the system.

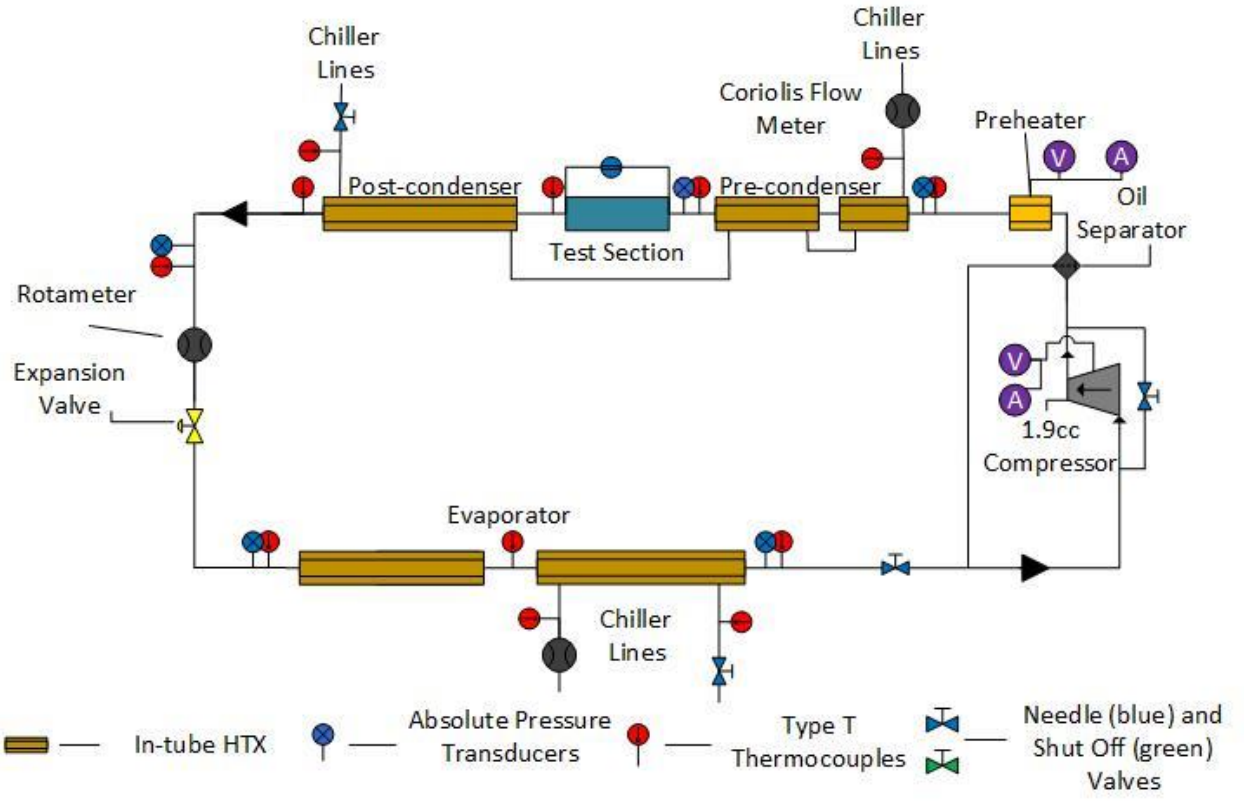

Figure 3.1 Schematic of vapor compression cycle designed for R134a and its alternatives

After exiting the oil separator, the refrigerant flows by an in-flow cartridge heater (Watlow FIREROD 1902) used to heat the refrigerant to a vapor with a superheat greater than 5°C to accurately set the state of the refrigerant prior to entering the condenser section. After passing the heater, the refrigerant enters the pre-condenser consisting of two tube-in-tube heat exchangers in series, in which refrigerant flows through the inner tube and water flows through the annulus in a counter-flow configuration. A recirculating chiller (Neslab ThermoFlex 2500) with a valve controls the water flow and temperature, and a Coriolis flow meter (Micro Motion 5700) measures the water mass flow rate. Type T thermocouples (Omega TMQSS-116U-6) measure the inlet and outlet temperatures of the water. The temperature (Omega TMQSS-116U-6) and pressure (Omega PX309-300A5V) of the refrigerant are measured at the inlet and outlet of the pre-condenser section. Following the pre-condensers, the refrigerant enters a copper test section with seven 0.95-

mm parallel channels, as described in Section 3.2. The refrigerant leaves the test section and passes through two more tube-in-tube heat exchangers; these post-condensers ensure that the refrigerant is fully subcooled before entering the rotameter.

The high-pressure, subcooled liquid refrigerant enters a four-tube rotameter (Omega FL-4SB-40C-40ST-39ST-39G-PTFE) that measures the volumetric flow rate of the refrigerant. The volumetric flow rate is converted to mass flow rate using the calibrations conducted for R134a, R513A, and R450A (Section 3.3). Only the smallest rotameter tube was used. Immediately after exiting the rotameter, the refrigerant passes through a manual expansion valve (Swagelok SS-SS4) and subsequently the low-pressure, liquid-vapor mixture refrigerant enters the evaporator, which consists of two counterflow tube-in-tube heat exchangers (i.e., refrigerant in the inner tube and water in the annulus). A second recirculating chiller (Neslab RTE-111) controlled the water flow and temperature. The refrigerant leaves the evaporator and reenters the compressor.

3.2 Test section

The test section is a machined coupon and heat flux block made from oxygen-free copper as discussed in Derby et al. [135]. The coupon consists of seven channels, each with a height of 0.98 mm and a width of 0.93 mm, resulting in a hydraulic diameter of 0.95 mm. The wall thickness between each channel is 0.5 mm; the length of the test section is 100 mm. The coupon contains an inlet and outlet header. Based on simulations conducted by Derby et al. [92, 135], the heat transfer in the inlet header is equal to twice the heat transfer coefficient of the middle segment and the outlet header is equal to the heat transfer coefficient of the middle segment.

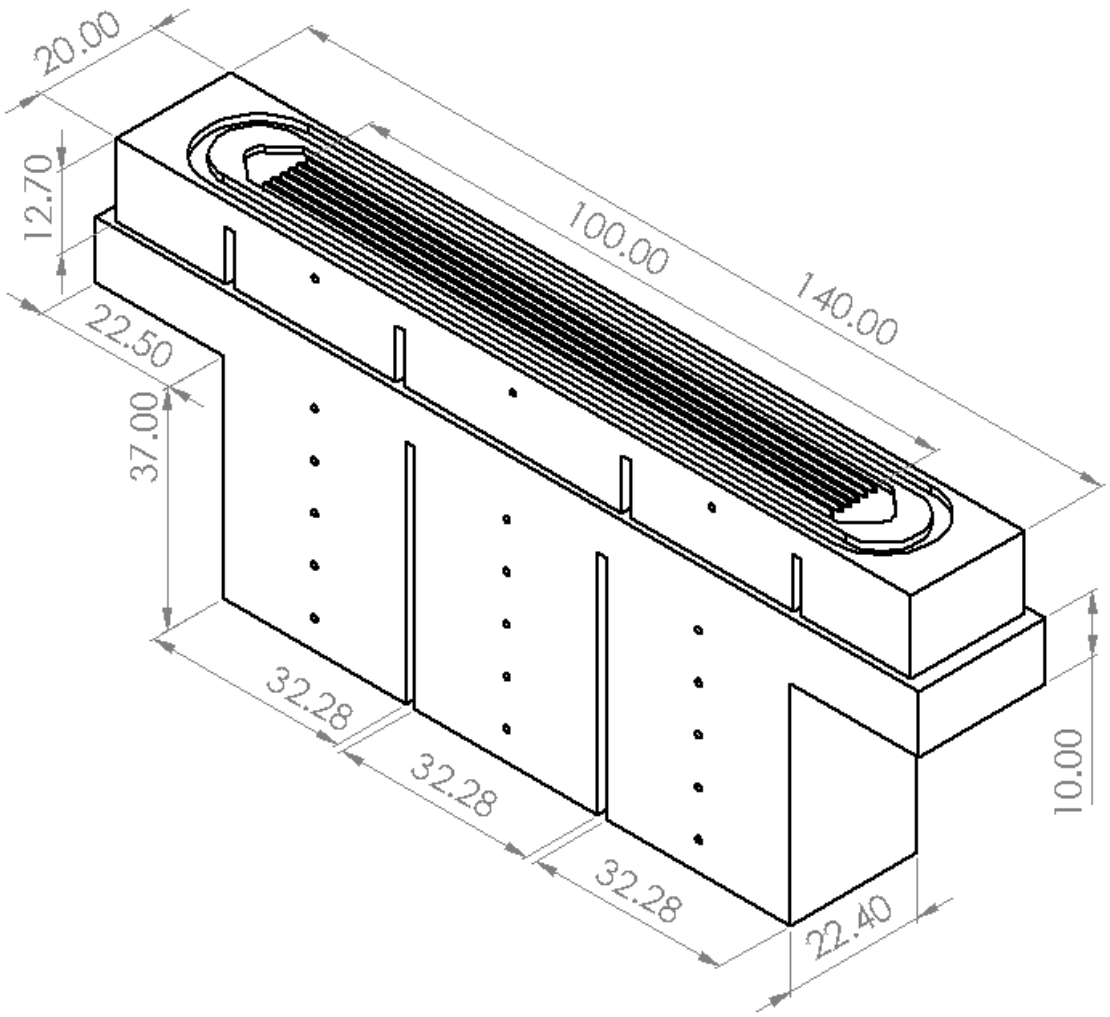

Figure 3.2 Schematic of test section assembly showing square channel test coupon and three segment heat flux block

The heat flux block is used to measure to heat flux leaving the bottom surface of the coupon. The heat flux block is comprised of three segments to reduce axial conduction [92]. Each segment consists of five 1-mm-diameter thermocouples, the first 8 mm from the top surface of the heat flux block and each one 8 mm lower in the y-axis. These type T thermocouples (Omega TJ36-CPSS-040U-6) aligned to the center of each segment measure the heat flux leaving the refrigerant. Wall temperature is measured by a thermocouple in the coupon located 3 mm from the channel bottom. Thermal paste (Arctic Silver 5) is used between the coupon and the block to reduce the contact resistance. A stainless-steel cooling block with a serpentine channel below the heat flux

block is used to have a constant heat flux boundary condition for cooling the refrigerant. A layer of thermal paste is used between the copper block and the cooling block. The test section is clamped together using six bolts.

3.3 Rotameter calibration

The rotameter was calibrated for R134a, R513A, and R450A using the calibration apparatus shown in Figure 3.2. The calibration apparatus consisted of two pressure vessels with the rotameter and a Coriolis flow meter (Micro Motion 5700) between them. The pressure vessel on the downstream side of the rotameter was put in a plastic bucket filled with ice water and salt to greatly lower its temperature. The system was charged with refrigerant and the downstream pressure vessel was cooled for three to four hours before data collection. A shutoff value kept the two vessels separate. The built-in valves of the rotameter adjusted the flow rate; shutoff valves kept all rotameter tubes closed except the one being calibrated. To calibrate, the flow shutoff valve was opened for a few seconds, long enough for the rotameter float to reach maximum height. The maximum rotameter reading and Coriolis reading were recorded. Adjusting for the next point, the process was repeated. Each tube was calibrated using 8 – 10 data points, depending on what was able to be obtained. The points were plotted in Excel and a linear calibration equation is calculated. The calibration curves for R134a, R513A and R450A are presented in Figures 3.3, 3.4, and 3.5, respectively. Because of the size of the compressor, only the smallest flow tube was needed for the system; therefore, only the smallest tube calibration curves are presented here.

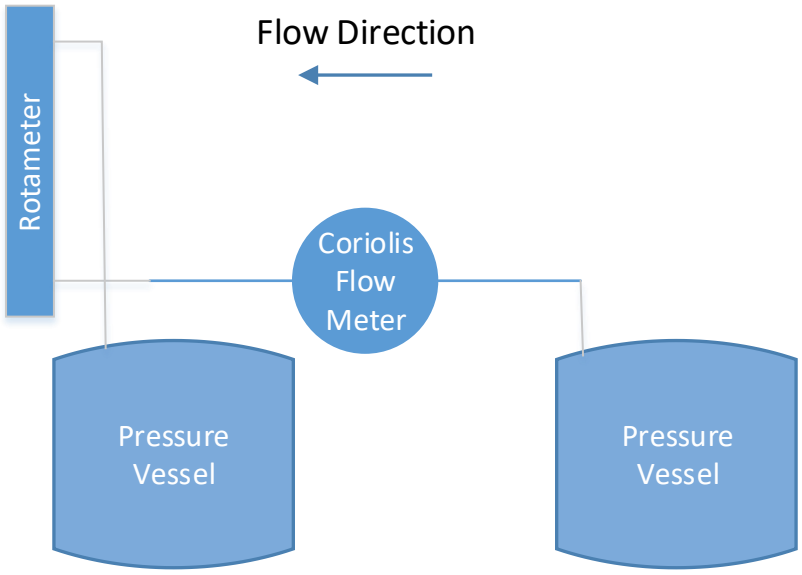

Figure 3.3 Schematic of rotameter calibration apparatus

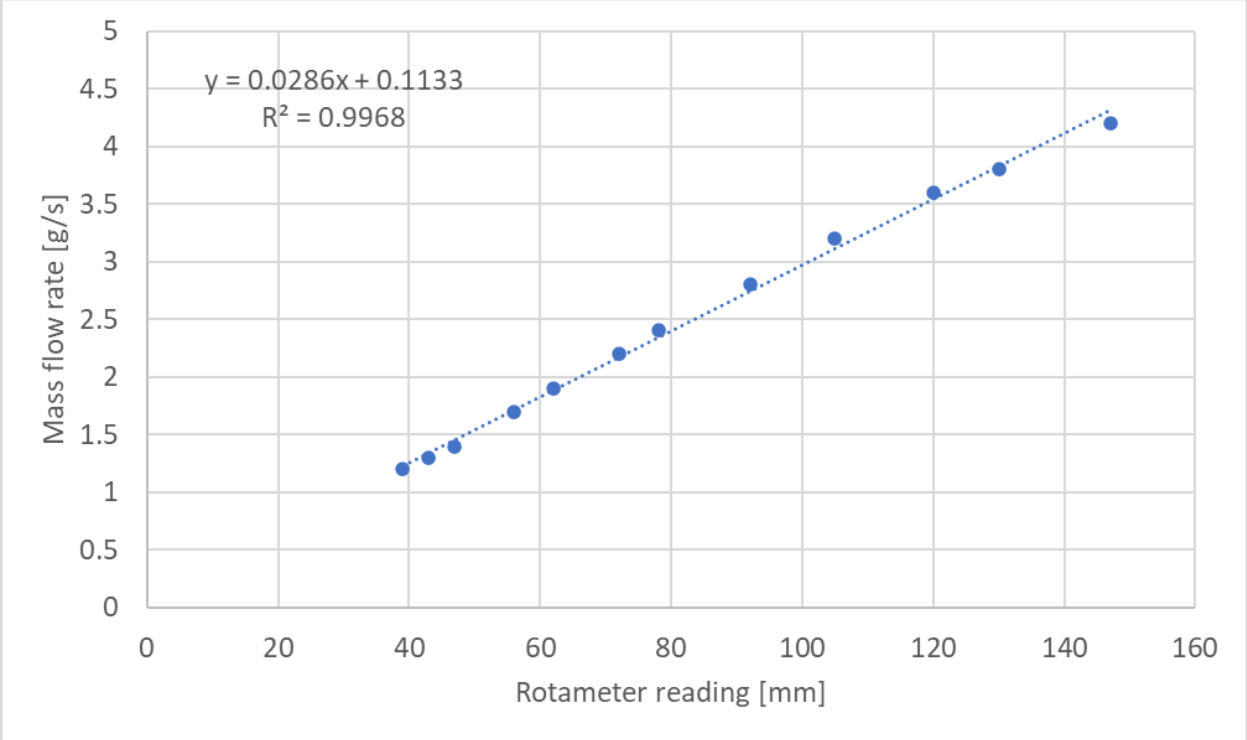

Figure 3.4 Rotameter tube #1 calibration curve for R134a

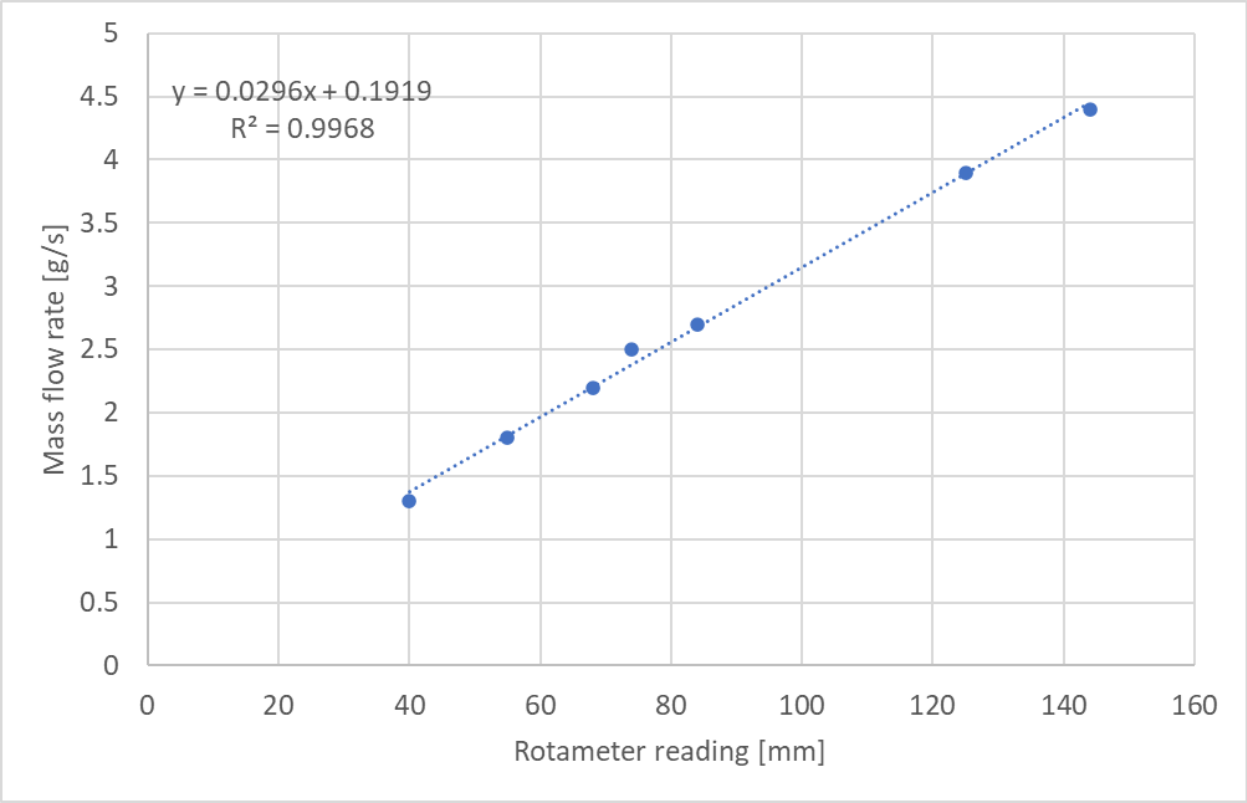

Figure 3.5 Rotameter tube #1 calibration curve for R513A

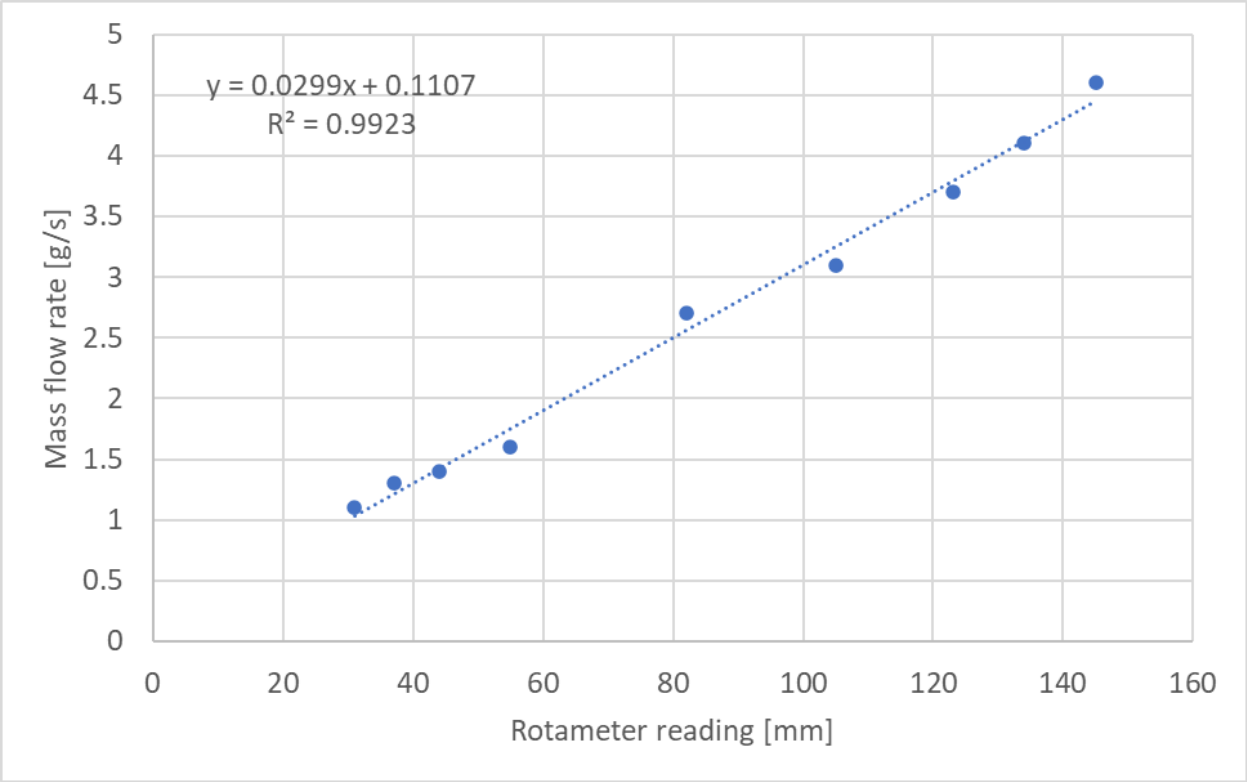

Figure 3.6 Rotameter tube #1 calibration curve for R450A

3.4 Data reduction procedure

Single phase and two-phase data reduction procedures are discussed in the following sections.

3.4.1 Single-phase data reduction

Single phase experiments collected data for energy balances and Nusselt numbers for R134a, R513A, and R450A to validate the system. The pre-condenser sub-cools the refrigerant entering the test section at least 5°C. The refrigerant is cooled at least 10°C across the test section for each experiment. The heat leaving the refrigerant across the test section is calculated by

$$\dot{Q}_{ref} = \dot{m}_{ref} c_{p,ref} (T_{in} - T_{out}) \tag{3.1}$$

where $\dot{m}_{ref}$ is the refrigerant mass flow rate, $c_{p,ref}$ is the specific heat capacity of the refrigerant, T_{in} is the temperature of the refrigerant entering the test section, and T_{out} is the temperature of the

refrigerant leaving the test section. The heat entering the heat flux block is calculated from the thermocouple measurements. The total block heat is calculated as

$$\dot{Q}_{block} = \dot{Q}_{header,in} + \dot{Q}_1 + \dot{Q}_2 + \dot{Q}_3 + \dot{Q}_{header,out} \tag{3.2}$$

where $\dot{Q}_i$ is the heat transfer in each block segment, $\dot{Q}_{header,i}$ is the heat transfer in the inlet header of the test section, and $\dot{Q}_{header,o}$ is the heat transfer in the outlet header of the test section. The heat transfer in each block segment is calculated by

$$\dot{Q}_i = q''_{block} A_{block} \tag{3.3}$$

where q''_{block} is the heat flux through each block segment and A_{block} is the cross-sectional area of the corresponding block segment. The heat flux through each block is calculated using Fourier's Law,

$$q''_{block} = -k_{cu} \frac{dT}{dy} \tag{3.4}$$

where k_{cu} is the thermal conductivity of copper and $\frac{dT}{dy}$ is the temperature gradient in the vertical y axis of each block segment. The temperature gradient is measured for each segment using a linear regression of the form

$$\frac{dT}{dy} = \frac{\sum(y_i - \bar{y})(T_i - \bar{T})}{\sum(y_i - \bar{y})^2} \tag{3.5}$$

where y_i is the distance in the y axis vertically down of the ith thermocouple from the top of the heat flux block, T_i is the measured temperature of the ith thermocouple, $\bar{y}$ is the average distance in the y axis vertically down, and $\bar{T}$ is the average measured temperature of the segment. The heat loss in the headers was modeled previously in Derby et al. [135] and calculated as

$$\dot{Q}_{header} = h_{header} A_{header} \left(T_{wall} - T_{fluid}\right) \tag{3.6}$$

where h_{header} is the header heat transfer coefficient, A_{header} is the header area, T_{wall} is the assumed header wall temperature, and T_{fluid} is the assumed refrigerant temperature in the header. The header fluid-wall temperature differences were found to be equal to the fluid-wall temperature differences of the corresponding segments, i.e., the first segment for the inlet and the third segment for the outlet; the header heat transfer coefficients were calculated as discussed in Section 3.2. The header area was measured as 6.75E-5 m^2 [92, 136].

The single-phase heat transfer coefficient is calculated by

$$h = \frac{q''_{ch}}{T_{fluid} - T_{wall}} \tag{3.7}$$

where q''_{ch} is the heat flux of the test section channel, T_{fluid} is the temperature of the refrigerant, and T_{wall} is the temperature of the channel wall. The fluid temperature is the average of the inlet and outlet measured fluid temperatures since the heat transfer coefficient is calculated from the center of the channel. The heat flux in the channel is calculated from the energy balance between the heat leaving the test section channel segment and the corresponding block segment:

$$q''_{ch} A_{s,ch} = q''_{block} A_{block} \tag{3.8}$$

where $A_{s,ch}$ is the surface area of the test section channel segment. The thermocouple measuring the wall temperature is 3 mm below the surface, so the wall temperature is extrapolated using the wall thermocouple plus the five thermocouples used to calculate the heat flux in the block. The measured wall temperature is less than 0.15°C from the measured wall temperature. The refrigerant Nusselt number is

$$Nu = \frac{hD}{k_{l,ref}} \tag{3.9}$$

where *h* is the second segment single phase heat transfer coefficient, *D* is the hydraulic diameter of the test section channel, and $k_{l,ref}$ is the refrigerant liquid thermal conductivity at the second segment of the test section. Properties were calculated using the refrigerant fluid temperature.

3.4.2 Condensation data reduction

The condensation heat transfer coefficient is calculated by

$$h = \frac{q''_{ch}}{T_{fluid} - T_{wall}} \tag{3.10}$$

The fluid temperature of two-phase condensation is the saturation temperature for azeotropic fluids (i.e., R134a, and R513A) and the bubble point temperature for zeotropic fluids (i.e., R450A). Because of the temperature glide of R450A across the liquid-vapor region, the fluid temperature is a function of pressure and quality. In two-phase flow, the first and third segments are influenced by entrance and exit effects; therefore, the only segment used for measuring refrigerant condensation heat transfer coefficients is the middle segment. A linear pressure drop across the test section is assumed for calculating the fluid pressure used for calculating fluid temperature; the fluid pressure for calculating the heat transfer coefficient is the average of the inlet and outlet pressure

In a similar way to the single-phase experiments, an energy balance beginning at the entrance of the preheater is used to calculate each segments' quality. The total water side heat transfer is calculated using

$$\dot{Q}_{pre} = \dot{m}_{water} c_{p,water} \left(T_{water,out} - T_{water,in}\right) \tag{3.10}$$

where $\dot{m}_{water}$ is the mass flow rate of the preheater annulus water flow, $c_{p,water}$is the specific heat capacity of water, and $T_{water,in}$ and $T_{water,out}$ are the measured water temperatures at the inlet and outlet of the preheater, respectively. Since the refrigerant enters the preheater as a

superheated vapor, the enthalpy of the refrigerant is found from the temperature and pressure at the inlet of the preheater. The enthalpy at the exit of the preheater, or the inlet of the test section, is found by

$$i_{in} = i_{pre} - \frac{\dot{Q}_{pre}}{\dot{m}_{ref}} \tag{3.11}$$

where i_{pre} is the enthalpy of the superheated vapor at the inlet of the precondenser. Because of the heat loss in the header of the test section, the heat transfer coefficient of the header is calculated the same way as the single-phase experiments. The enthalpy after the inlet header is calculated from the equation

$$\dot{Q}_{header,in} = \dot{m}_{ref}\left(i_{in} - i_{header,in}\right) \tag{3.12}$$

where $i_{header,in}$ is the enthalpy after the inlet header, and $\dot{Q}_{header,in}$ is calculated from Equation 3.6. The enthalpy of the point after the first block segment is calculated using the equation

$$\dot{Q}_1 = \dot{m}_{ref}\left(i_{header,in} - i_A\right) \tag{3.13}$$

where $\dot{Q}_1$ is the heat transfer through the first block segment and i_A is the enthalpy after the first block segment. The enthalpy at the center of the first block segment is calculated by the average between the enthalpy at the beginning and end of the segment:

$$i_1 = \frac{i_{header,in} + i_A}{2} \tag{3.14}$$

The enthalpy in the middle of segments 2 and 3 are calculated in a similar fashion using energy balances.

3.5 Experimental uncertainties

Experimental uncertainties (i.e., experimental measurement error) were calculated using a propagation of uncertainty analysis as described by Kline and McClintock [137]. The heat transfer coefficient uncertainty was calculated as

$$\omega_h = \sqrt{\left(\frac{\partial h}{\partial q"_{block}}\right)^2 \omega_{q"_{block}}^2 + \left(\frac{\partial h}{\partial A_{block}}\right)^2 \omega_{A_{block}}^2 + \left(\frac{\partial h}{\partial A_{ch}}\right)^2 \omega_{A_{ch}}^2 + \left(\frac{\partial h}{\partial T_{fluid}}\right)^2 \omega_{T_{fluid}}^2 + \left(\frac{\partial h}{\partial T_{wall}}\right)^2 \omega_{T_{wall}}^2} \quad (3.16)$$

The temperature gradient uncertainty in the blocks used to measure heat flux was calculated using the equation presented in Kedzierski and Worthington [138] as the following

$$\omega_{\frac{dT}{dy}} = \sqrt{\omega_T^2 + \left(\frac{q"_{block} D_{tc}}{6k_{cu}}\right)^2} \sqrt{\frac{1}{\sum_{i=1}^{N}(y_i - \bar{y})^2}} \quad (3.17)$$

where D_{tc} is the thermocouple hole diameter, k_{cu} is the thermal conductivity of copper, y_i is the vertical location of each thermocouple location used in the heat flux calculation, and $\bar{y}$ is the average thermocouple location. The uncertainty of all machined part lengths is half on the finest reading of the calipers used to measure the distances, corresponding to 0.005 mm. The uncertainty of the absolute pressure transducers was 0.25% full scale, corresponding to 0.75 psi. The uncertainty of the differential pressure transducer was also 0.25% full scale, corresponding to 0.075 psi. The uncertainty of the calibrated type T thermocouples was 0.2°C. The wall temperature was extrapolated so the uncertainty of the wall temperature was calculated using

$$\omega_{T_{wall}} = \sqrt{\omega_T^2 + \left(y\omega_{\frac{dT}{dy}}\right)^2} \quad (3.18)$$

where the y is the distance from the bottom of the test section to the thermocouple hole (i.e., 3 mm). The fluid temperature uncertainty is based on the saturation pressure for R134a and R513A and saturation pressure and quality for R450A. For the mass flux, the uncertainty of the rotameter is 2% full scale, which corresponds to 0.0858 g/s for R134a, 0.0888 g/s for R513A, and 0.0897 g/s for R450A. The heat transfer coefficient uncertainties for all experiments were ±6.3 – 21.2%, with an average of ± 9.8%. The heat transfer coefficient uncertainties of R134a were ±6.3 – 10.8%,

with an average of ± 7.8%. The heat transfer coefficient uncertainties of R513A were ±8.9 – 21.2%, with an average of ± 11.8%. The heat transfer coefficient uncertainties of R450A were ±8.0 – 12.1%, with an average of ± 9.6%.

The uncertainty of quality is calculated from the energy balances used to calculate the enthalpies. The quality uncertainty is calculated as

$$\omega_x = \sqrt{\left(\frac{\partial x}{\partial i_2}\right)^2 \omega_{i_2}^2 + \left(\frac{\partial x}{\partial i_l}\right)^2 \omega_{i_l}^2 + \left(\frac{\partial x}{\partial i_{lv}}\right)^2 \omega_{i_{lv}}^2} \tag{3.19}$$

where i_2 is the enthalpy in the middle of the second test section segment, i_L is the saturated liquid enthalpy and i_{LV} is the latent heat of vaporization. The uncertainty of i_2 is calculated as

$$\omega(i_2) = \sqrt{\begin{aligned}&\left(\frac{\partial i_2}{\partial i_{pre}}\right)^2 \omega_{i_{pre}}^2 + \left(\frac{\partial i_2}{\partial \dot{Q}_{pre}}\right)^2 \omega_{\dot{Q}_{pre}}^2 + \left(\frac{\partial i_2}{\partial \dot{Q}_{header,in}}\right)^2 \omega_{\dot{Q}_{header,in}}^2 \\ &+ \left(\frac{\partial i_2}{\partial \dot{Q}_1}\right)^2 \omega_{\dot{Q}_1}^2 + \left(\frac{\partial i_2}{\partial \dot{Q}_2}\right)^2 \omega_{\dot{Q}_2}^2 + \left(\frac{\partial i_2}{\partial \dot{m}_{ref}}\right)^2 \omega_{\dot{m}_{ref}}^2\end{aligned}} \tag{3.20}$$

where $\dot{Q}_1$ and $\dot{Q}_2$ are the heat transfer through the first two block segments.

Chapter 4 - Results and discussion

R134a, R513A, and R450A experimental condensation heat transfer coefficient results are presented. A single-phase validation was done using energy balances and single-phase Nusselt number correlations. The condensation heat transfer coefficient results are presented for R134a, R513A and R450A for three mass fluxes (i.e., 200, 350, and 500 kg/m^{2}s) for a quality range between 0.2 and 0.8. The mass fluxes selected covered the minimum and maximum capabilities of the compressor. The refrigerants are compared to three general correlations to show how well the correlations predict performance of the refrigerants.

4.1 Single-phase validation

R134a, R513A, and R450A single-phase energy balances are presented in Figure 4.1. The energy balance in the test section was between the heat transfer through the heat flux block and the heat transfer leaving the refrigerant. The energy balance shows good agreement between the two heat transfer rates, calculated by Equations 3.1 and 3.2, well within single phase uncertainties.

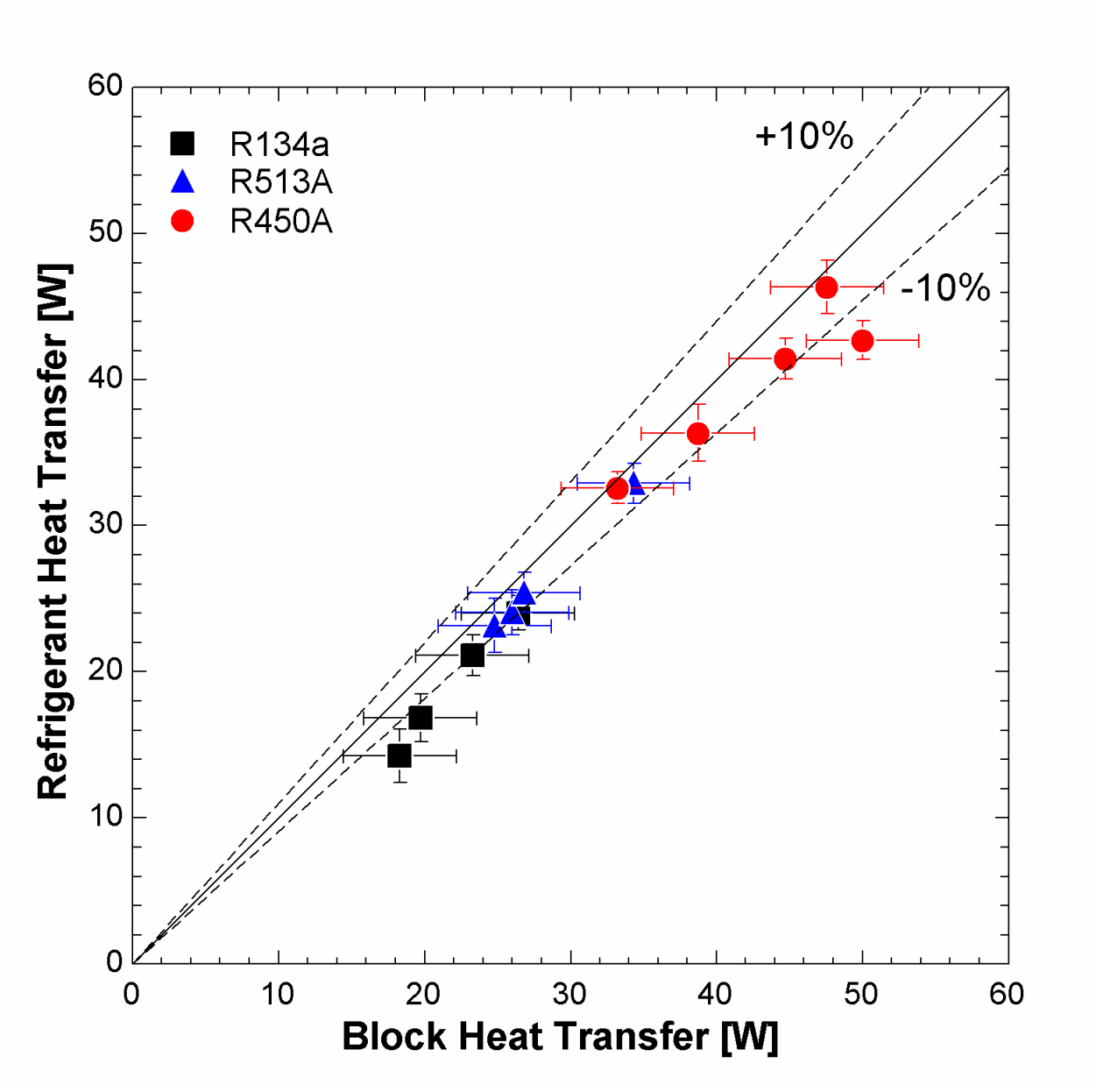

Figure 4.1 Single-phase energy balances of R134a, R513A, and R450A

Figure 4.2 shows the single-phase Nusselt numbers for R134a, R513A, and R450A. The refrigerants were compared to single-phase Nusselt number correlations. The data points within the laminar region (i.e., Re<2,000) were predicted using the Wibulswas [139] correlation, and the data points within the transition region (i.e., Re>2,000) were predicted using the Gnielinski [140]

correlation. The Nusselt numbers showed good agreement to the correlations. The energy balances and Nusselt numbers validated the data collection process.

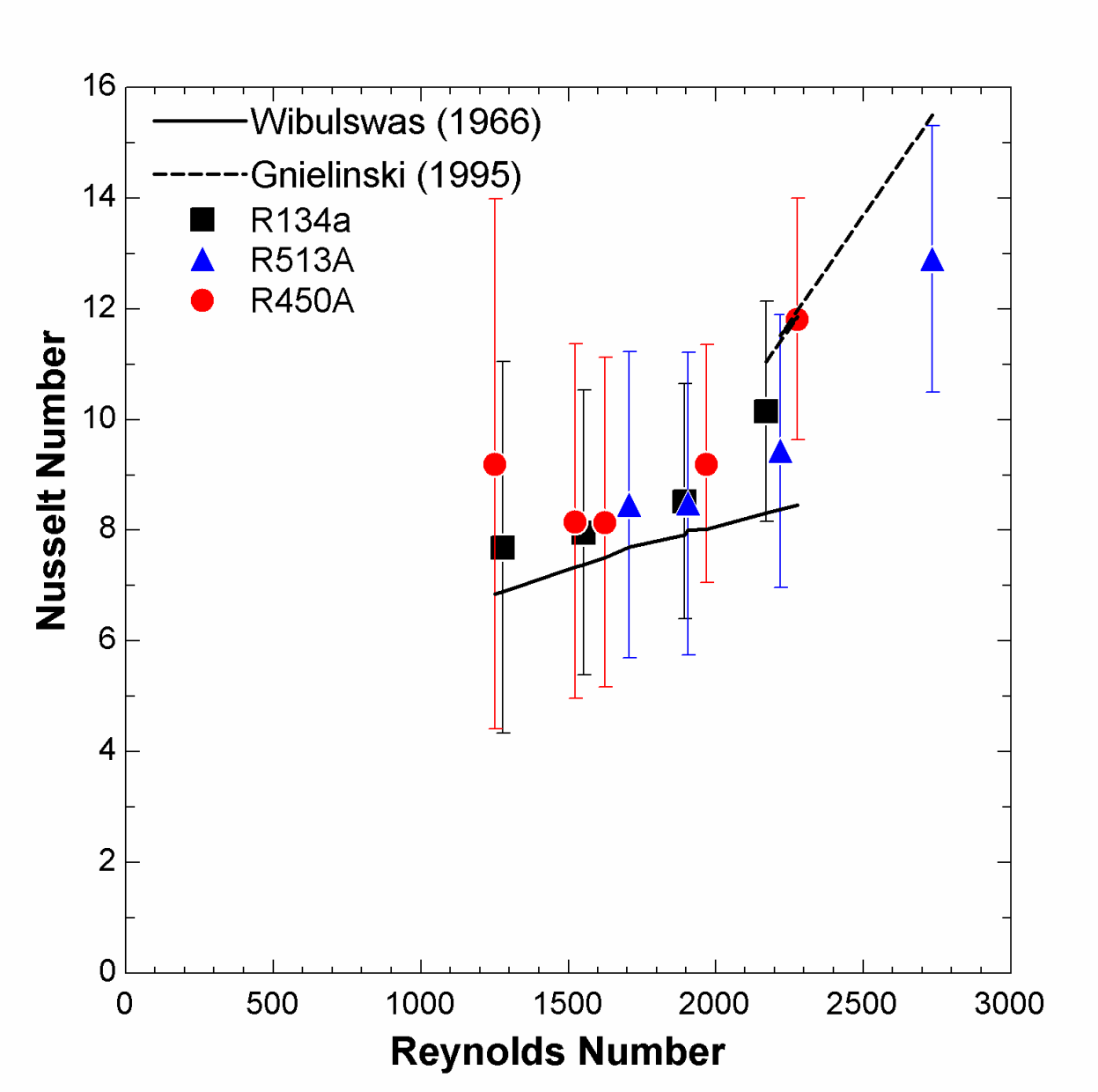

Figure 4.2 Single-phase Nusselt numbers of R134a, R513A, and R450A compared to single phase correlations

4.2 Condensation heat transfer coefficients

Condensation heat transfer coefficients were collected for R134a, R513A, and R450A. Figures 4.3, 4.4, and 4.5 show R134a, R513A, and R450A condensation transfer coefficients at

mass fluxes of 200, 350, and 500 kg/m^{2}s, respectively. All data were collected at a saturation temperature of 40°C±1°C. The saturation temperature was a function of the saturation pressure for R134a and R513A and a function of saturation pressure and quality for R450A due to its temperature glide. Overall, condensation heat transfer coefficients increase with increasing mass flux and quality.

R134a condensation heat transfer coefficients were generally higher than R513A and R450A in all three mass fluxes. This is consistent with most of the data in literature for R513A [60-62, 95] and R450A [121, 122]. The lower performance of R513A can be explained by the lower liquid thermal conductivity, lower latent heat of vaporization, and higher vapor density. The lower thermal conductivity creates a lower conductive effect through liquid phase. The higher vapor density creates lower velocities for a lower convective effect. At 40°C, the liquid thermal conductivity of R134a is 74.72 W/m K, the latent heat of vaporization of R134a is 163.0 kJ/kg, and the vapor density of R134a is 50.09 kg/m^3. At 40°C, the liquid thermal conductivity of R513A is 65.40 W/m K, the latent heat of vaporization of R513A is 142.6 kJ/kg, and the vapor density of R513A is 54.20 kg/m^3. The lower performance of R450A can be explained by lower thermal conductivity, lower latent heat of vaporization, and lower specific heat. All three properties make it harder for R450A carry and conduct heat. At 40°C, the liquid specific heat of R134a is 1.50 kJ/kg K. At 40°C, the liquid thermal conductivity of R450A is 70.76 W/m K, the latent heat of vaporization of R450A is 154.8 kJ/kg, and the liquid specific heat of R450A is 1.49 kJ/kg K.

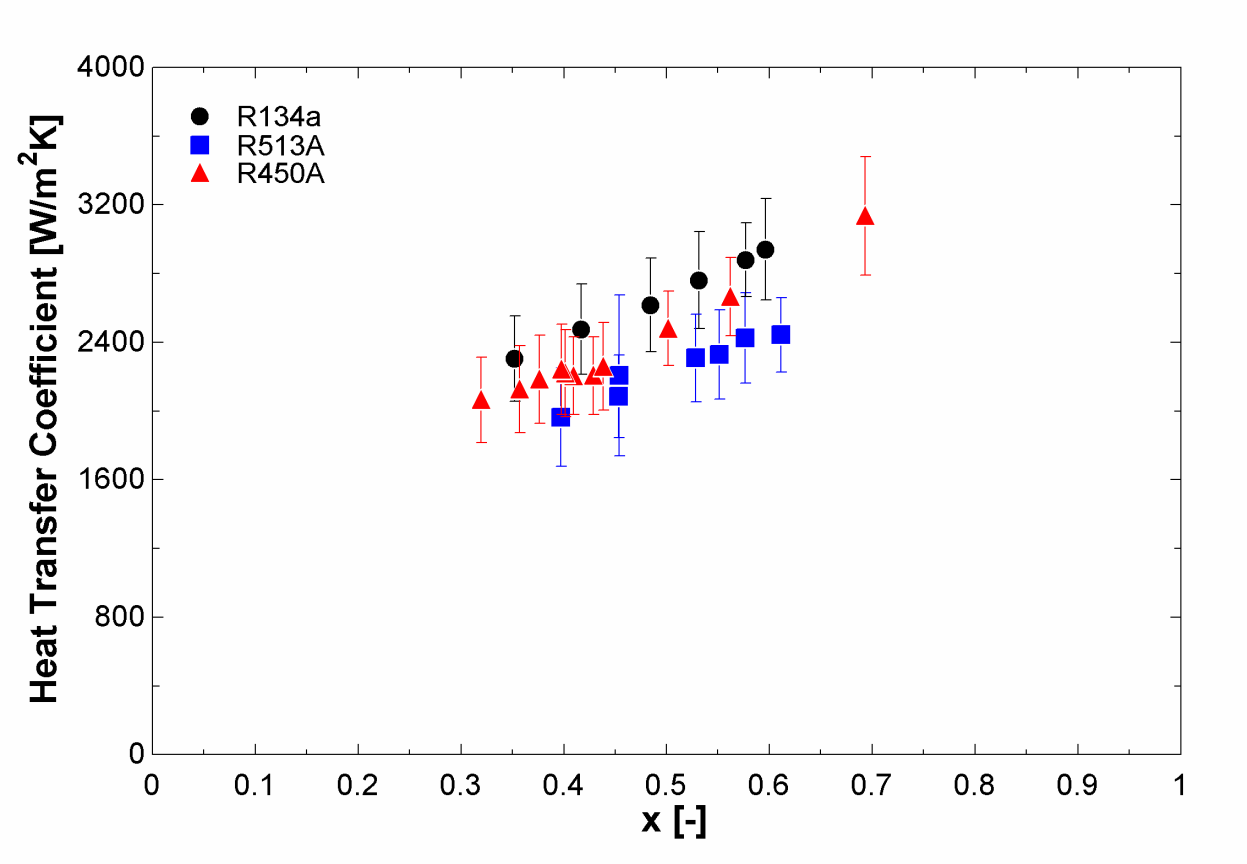

Figure 4.3 Condensation heat transfer coefficients versus quality for R134a, R513A, and R450A at a mass flux of 200 kg/m^{2}s and a temperature of 40°C

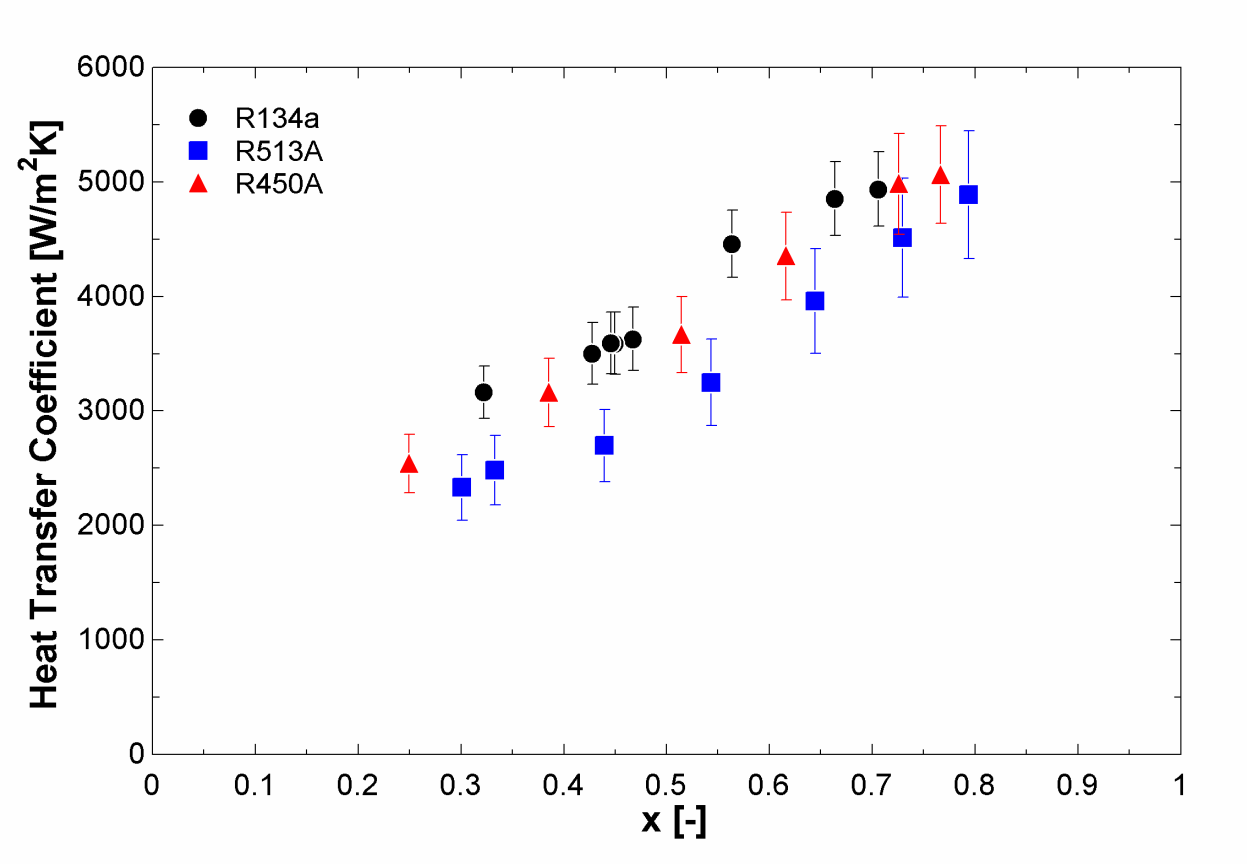

Figure 4.4 Condensation heat transfer coefficients versus quality for R134a, R513A, and R450A at a mass flux of 350 kg/m^{2}s and a temperature of 40°C

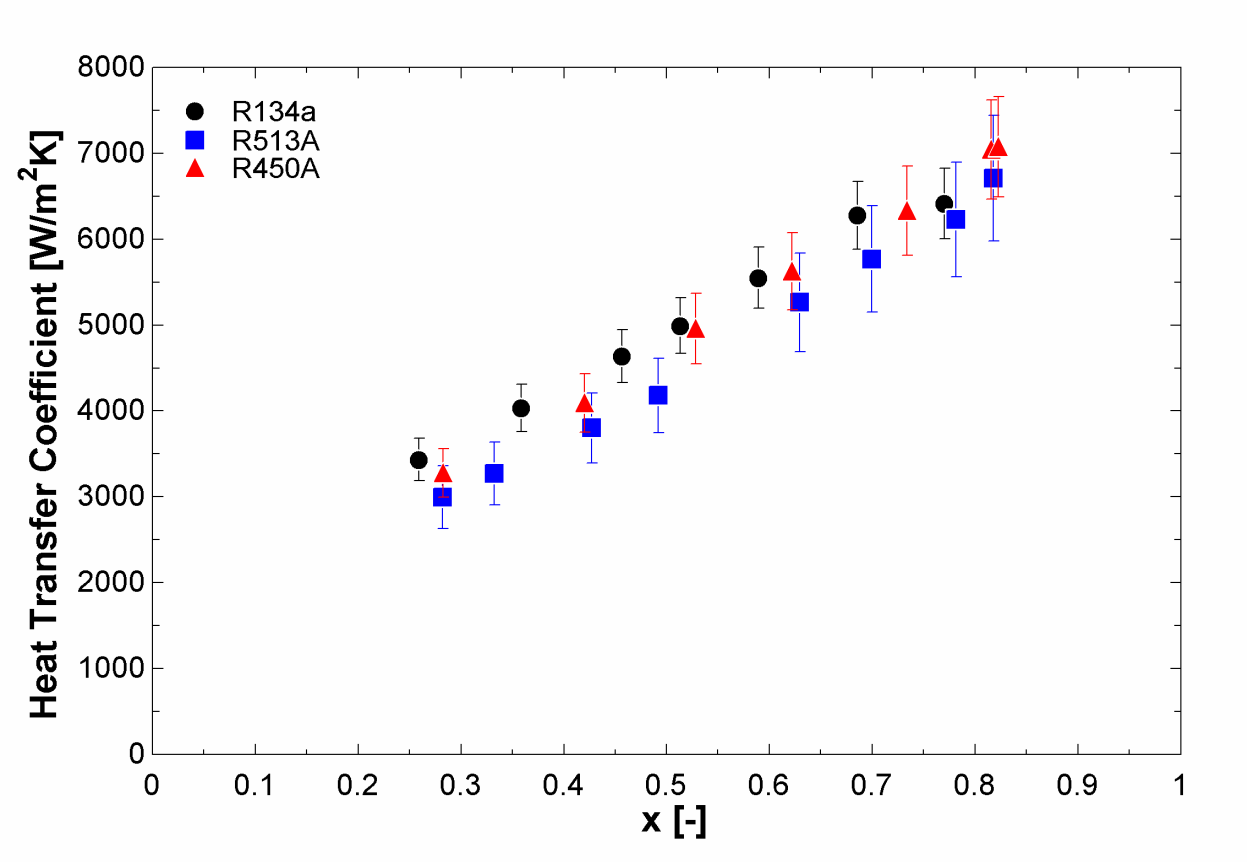

Figure 4.5 Condensation heat transfer coefficients versus quality for R134a, R513A, and R450A at a mass flux of 500 kg/m^{2}s and a temperature of 40°C

Due to the nature of experiments, direct comparison between the three refrigerants is difficult since it can be difficult to collect data at the exact same mass flux and quality for all three refrigerants. Because of this, a linear regression line was created from the R134a data for each mass flux. R134a heat transfer coefficients were calculated using the equation, and the R513A and R450A experimental data were compared to the calculated R134a value. The R^2 values for the R134a heat transfer coefficient curve fit equations are 0.997 (G=200 kg/m^{2}s), 0.968 (G=350 kg/m^{2}s), and 0.989 (G=500 kg/m^{2}s). Figure 4.6 presented the comparison for both R513A and R450A for all three mass fluxes. For a mass flux of 200 kg/m^{2}s, R513A showed heat transfer coefficients on average 17% (13.9 – 18.7%) less than R134a while the R450A data point at a quality of 0.69 was 1.4% lower than R134a, but the rest of the data was on average 8% (6.2 –

11.7%) lower than R134a. At a mass flux of 350 kg/m^{2}s, the R513A condensation heat transfer coefficient at a quality of 0.79 was 10.5% and trending away from R134a values at lower qualities to 25.6% at a quality of 0.44. R513A heat transfer coefficients below a quality of 0.4 were 19.2 – 19.7% lower than R134a. R450A heat transfer coefficients were on average 4.9% (2.4 – 8.7%) lower than R134a at mass flux of 350 kg/m^{2}s, with the biggest differences around a quality of 0.5. At the mass flux of 500 kg/m^{2}s, R513A heat transfer coefficients were on average 9.9% lower than R134a ranging from 2.6 to 16% at qualities of 0.82 and 0.28, respectively. R450A heat transfer coefficients were 2.4% lower on average than R134a with heat transfer coefficients that were 8.8% lower at low quality (i.e., 0.28) and heat transfer coefficients up to 2% higher than R134a at high quality (i.e., 0.82). Based on this analysis, R513A heat transfer coefficients were on average 15% lower than R134a; R450A heat transfer coefficients were typically 5% lower than R134a. The uncertainties of these refrigerants were large enough that it does affect the comparison between R134a, R513A, and R450A. the differences between R134a and R513A were large enough that R513A does show lower performance; however, the differences between R134a and R450A were typically around 5%, lower than the average uncertainties of R450A (i.e., 9.6%).

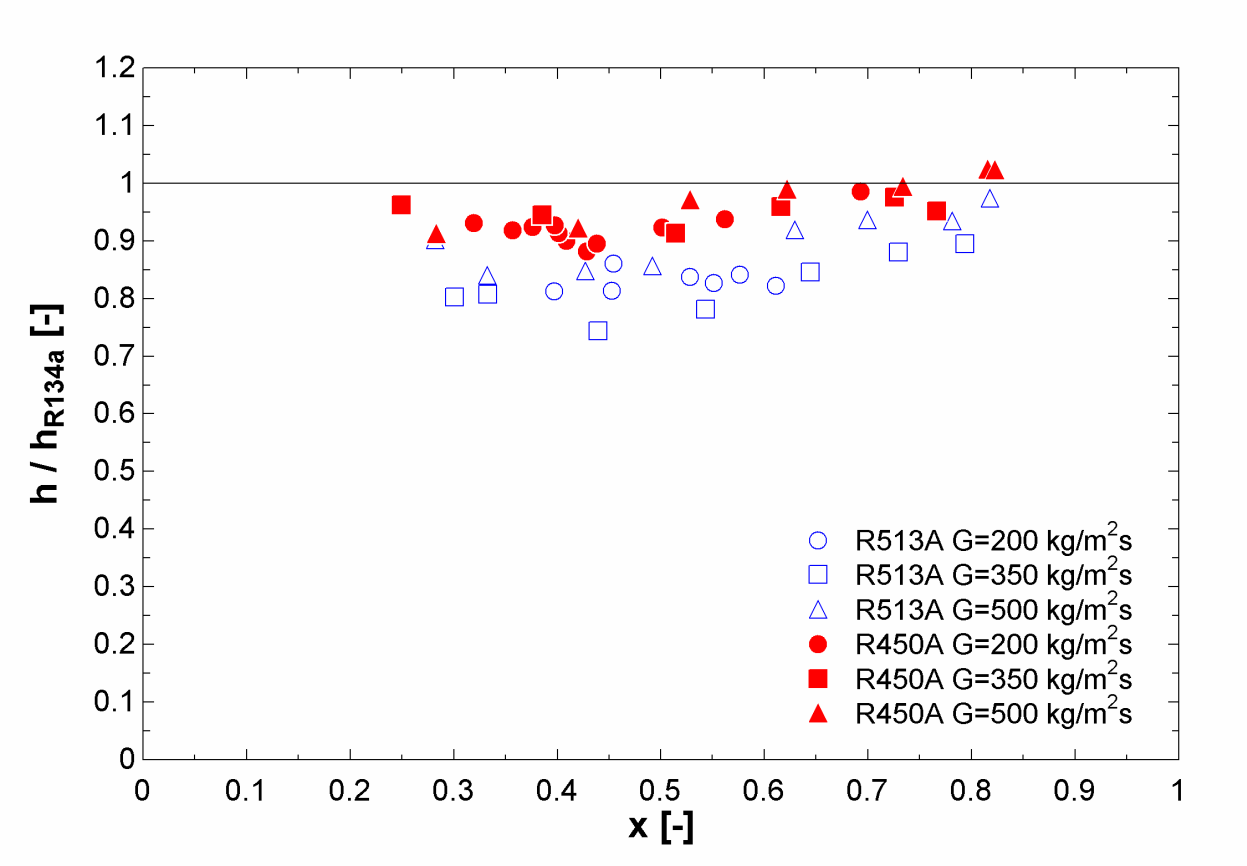

Figure 4.6 Comparison of R513A and R450A to R134a heat transfer coefficients for mass fluxes of 200, 350, and 500 kg/m^{2}s

4.3 Correlation comparison

R134a, R513A, and R450A condensation heat transfer coefficients were compared to general condensation correlations, Kim and Mudawar [133], Shah [132], and Cavallini et al. [129]. As shown in Figures 4.7, 4.8, and 4.9, all three correlations tended to overpredict the data. Figure 4.7 presents the experimental heat transfer coefficients versus the heat transfer coefficients predicted by the Kim and Mudawar [133] correlation (Eqns 2.1 and 2.2). The correlation shows good agreement with the experimental results with an overall mean average error (MAE) of 15.9%. The Kim and Mudawar [133] correlation predicted R134a the best; R450A had the largest MAE at 20%. Figure 4.8 presents the experimental heat transfer coefficients versus the heat transfer coefficients predicted by the Shah [132] correlation (Eqns 2.5 and 2.6). The Shah [132] correlation

also shows good agreement with the results with an overall MAE of 23.7%. The Shah [132] correlation predicts R134a the best and R513A the worst, though the differences were minimal. The Cavallini et al. [129] correlation (Eqns 2.3 and 2.4) predicted the data with an overall MAE of 23.7% as shown in Figure 4.9. The Cavallini et al. [129] MAE is the same as the Shah MAE because Shah incorporated the equation used by Cavallini et al. [27] for Regime 1; all the experimental data collected fell into Regime 1 of the Shah [132] correlation.

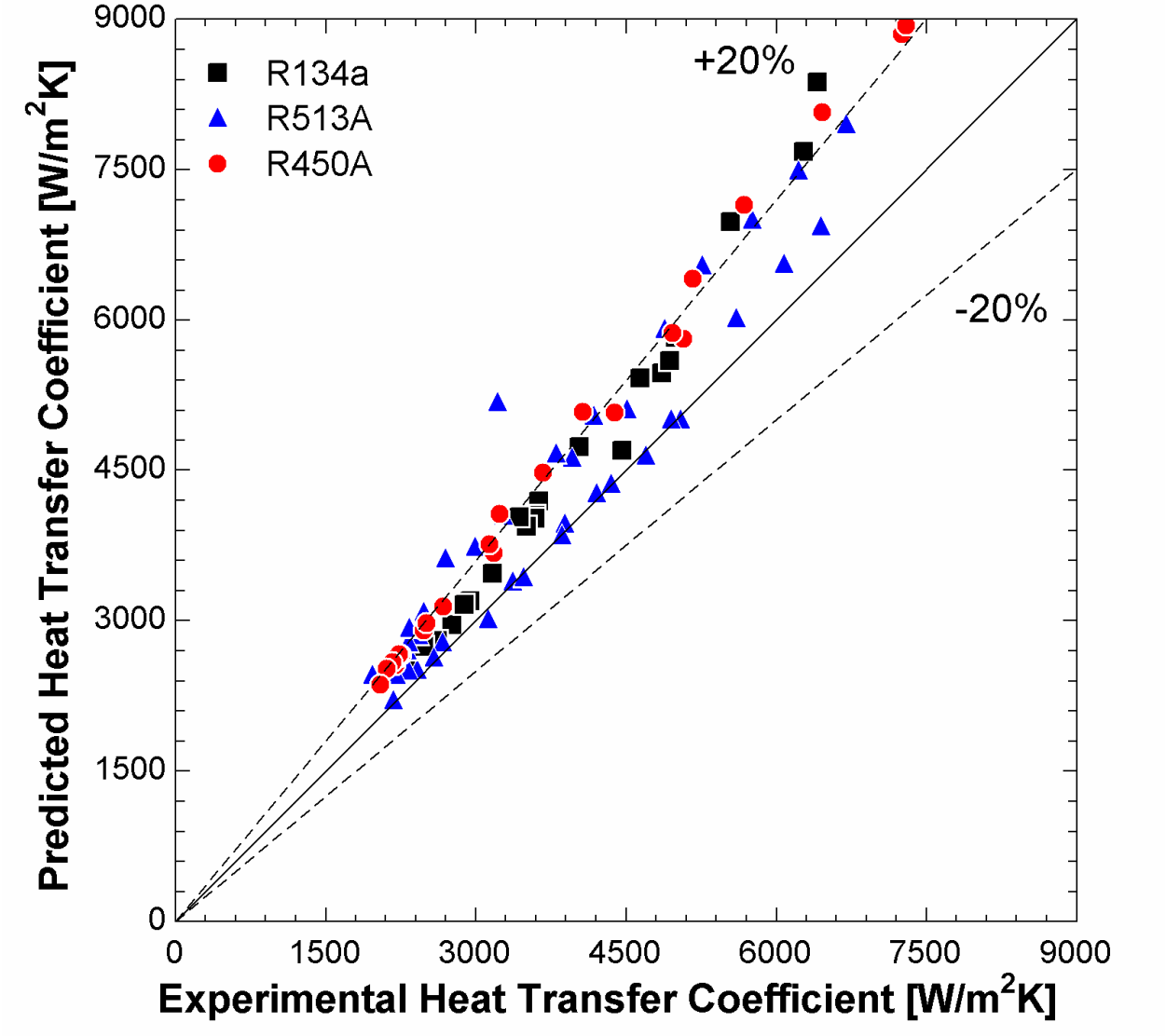

Figure 4.7 Experimental condensation heat transfer coefficients versus condensation heat transfer coefficients predicted by the Kim and Mudawar [133] correlation

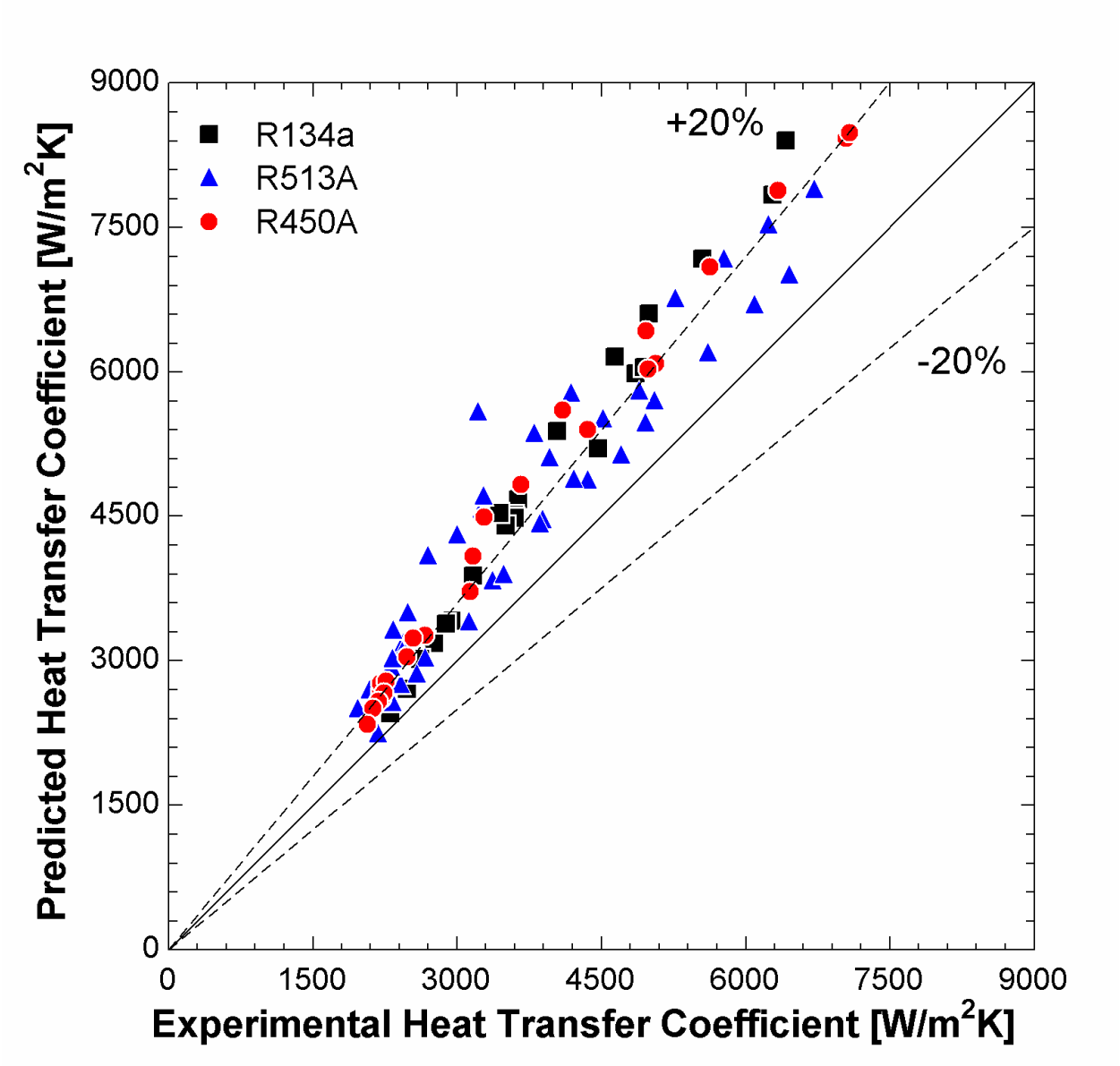

Figure 4.8 Experimental condensation heat transfer coefficients versus condensation heat transfer coefficients predicted by the Shah [132] correlation

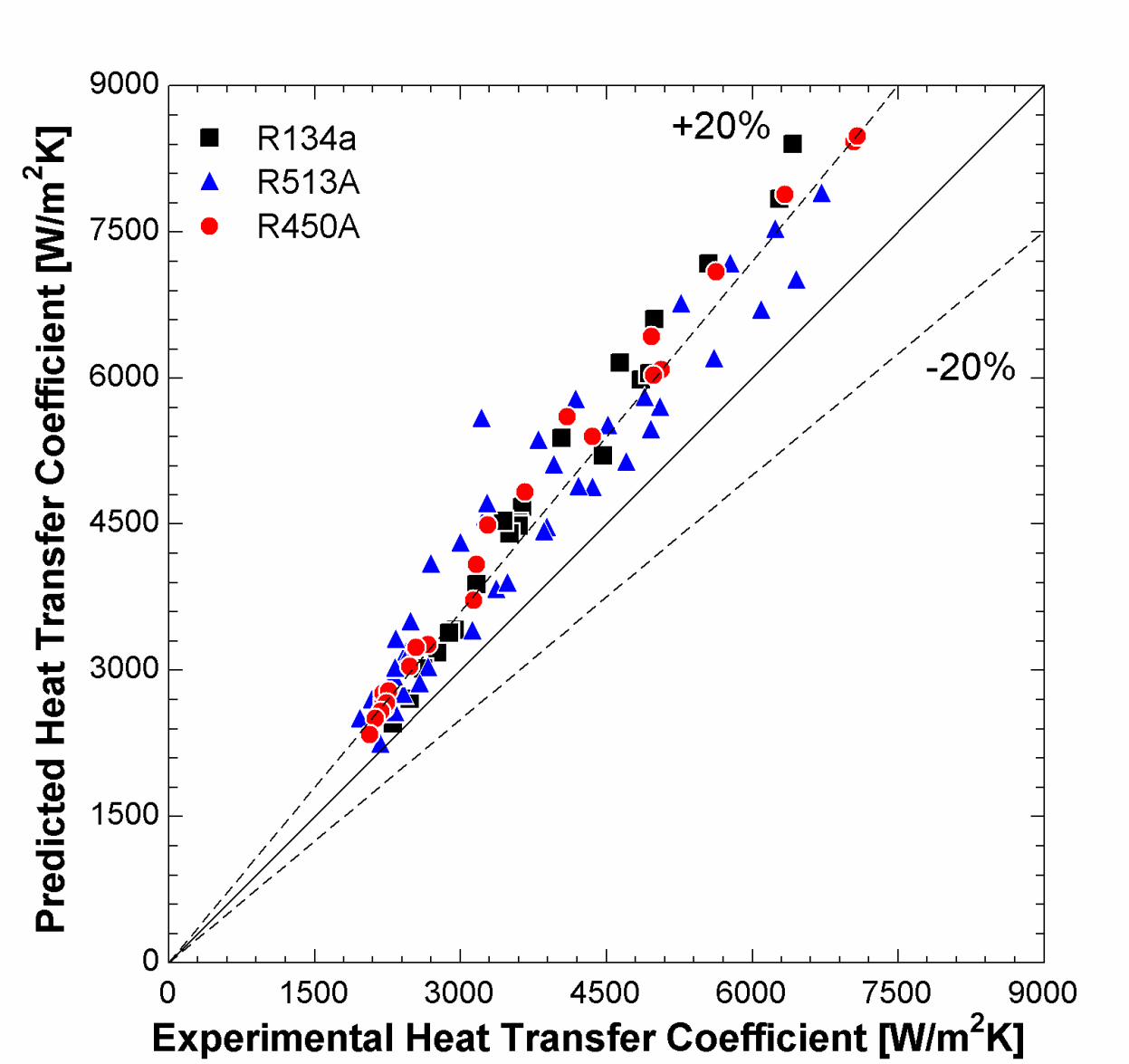

Figure 4.9 Experimental condensation heat transfer coefficients versus heat transfer coefficients predicted by the Cavallini et al. correlation

4.4 Condensation pressure drops

Condensation pressure drops are presented for R134a, R513A, and R450A at the same mass fluxes as the condensation heat transfer coefficients. Figures 4.10, 4.11, and 4.12 present the pressure drop versus quality for each mass flux. Pressure drop increases with increasing mass flux and quality for R134a, R513A and R450A. At a mass flux of 200 kg/m^{2}s, R513A pressure drops were about 5% lower than R134a; R450A pressure drops were marginally higher (i.e., less than

5%) than R134a. For a mass flux of 350 kg/m^{2}s, R513A pressure drops were about 10% lower than R134a while R450A pressure drops were comparable to R134a. At the highest mass flux (i.e., 500 kg/m^{2}s), R513A pressure drops were between 5 – 10% different with larger differences at high mass flux. R450A pressure drops were again comparable to R134a.

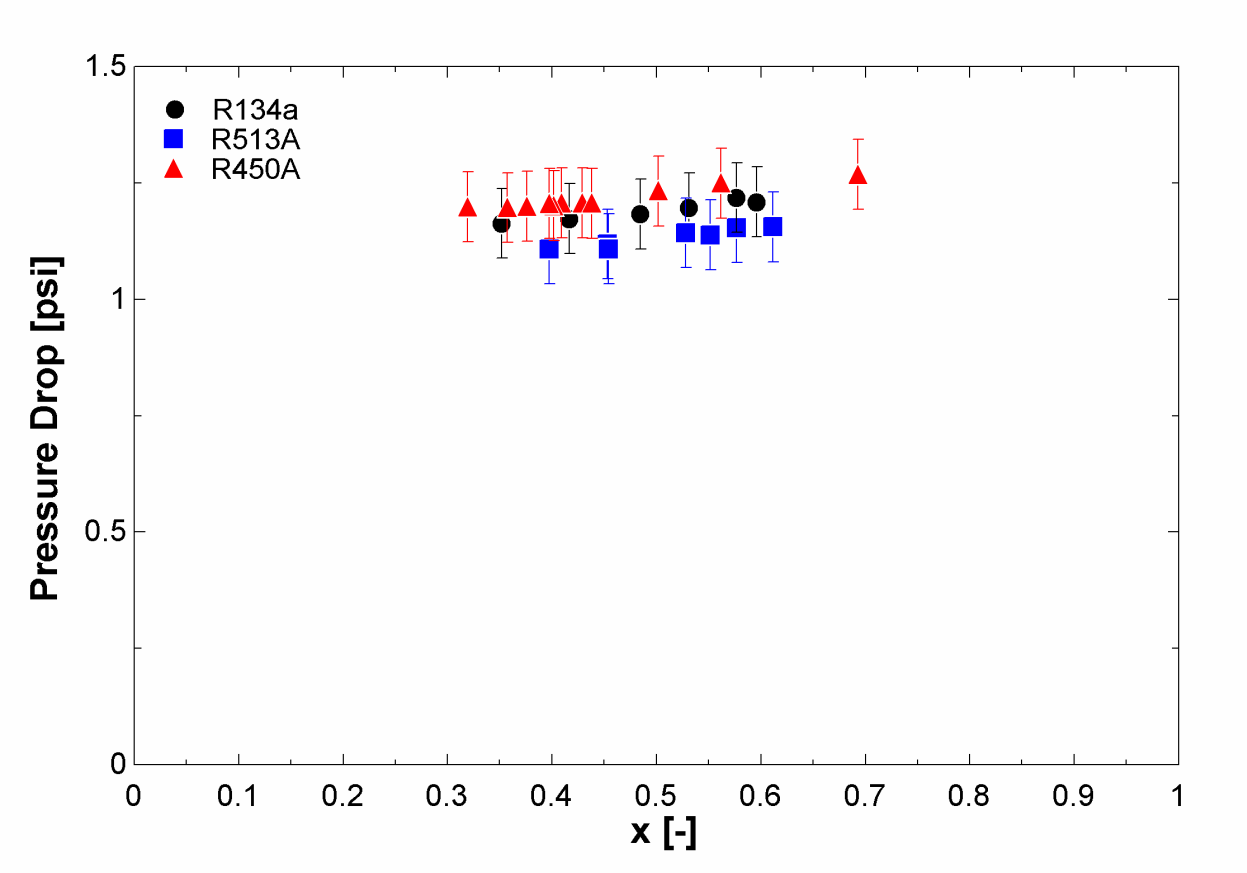

Figure 4.10 Pressure drop versus quality for R134a, R513A, and R450A at a mass flux of 200 kg/m^{2}s

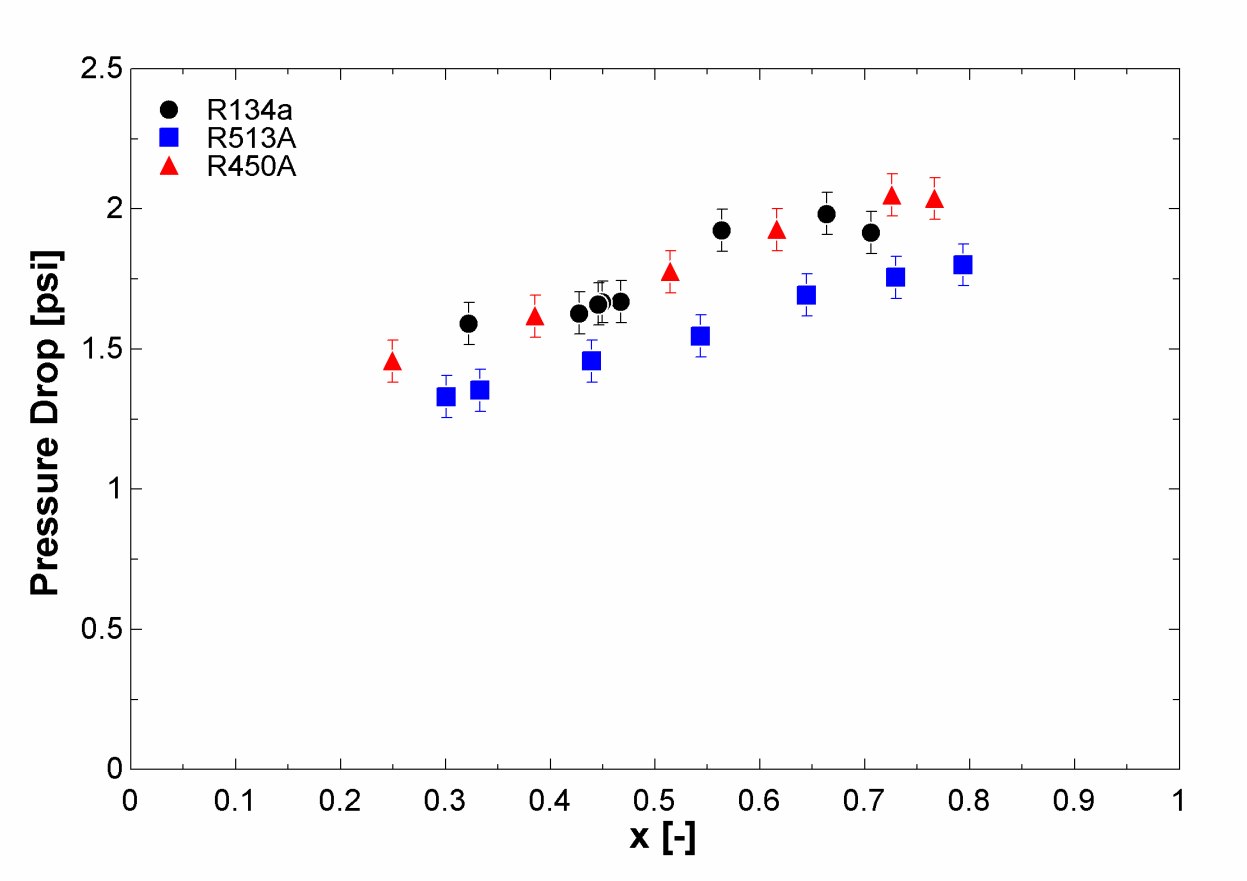

Figure 4.11 Pressure drop versus quality for R134a, R513A, and R450A at a mass flux of 350 kg/m^{2}s

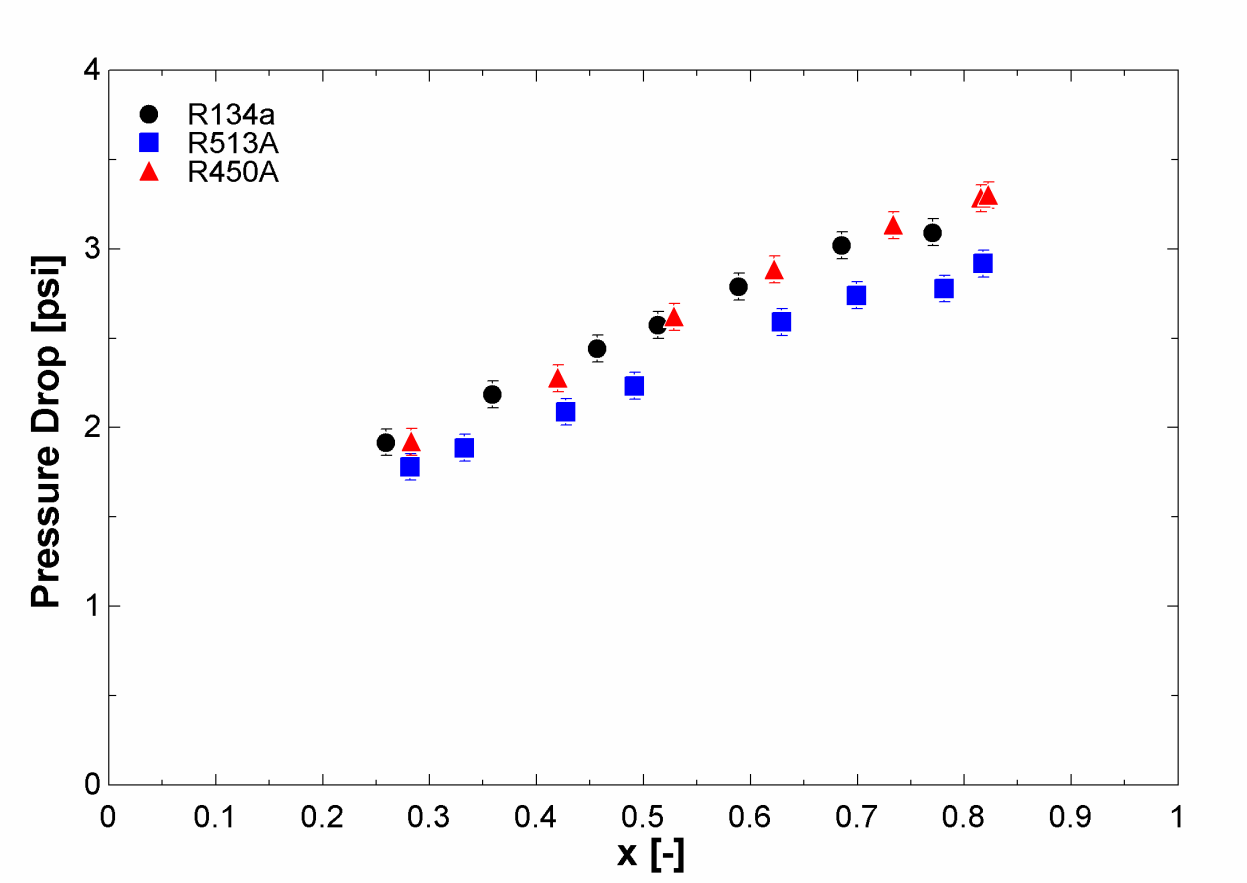

Figure 4.12 Pressure drop versus quality for R134a, R513A, and R450A at a mass flux of 500 kg/m^{2}s

The variance in pressure drops measured was investigated. The standard deviation of the pressure drop measurements for R134a, R513A, and R450A range between 0.011 psi and 0.078 psi. The higher standard deviations corresponded to higher mass fluxes. For the lower mass fluxes (i.e., 200 and 350 kg/m^{2}s), the pressure drop uncertainty is the larger measurement error; at the highest mass flux, the standard deviation is higher than the measurement uncertainty in some cases, but typically similar to the measurement uncertainty.

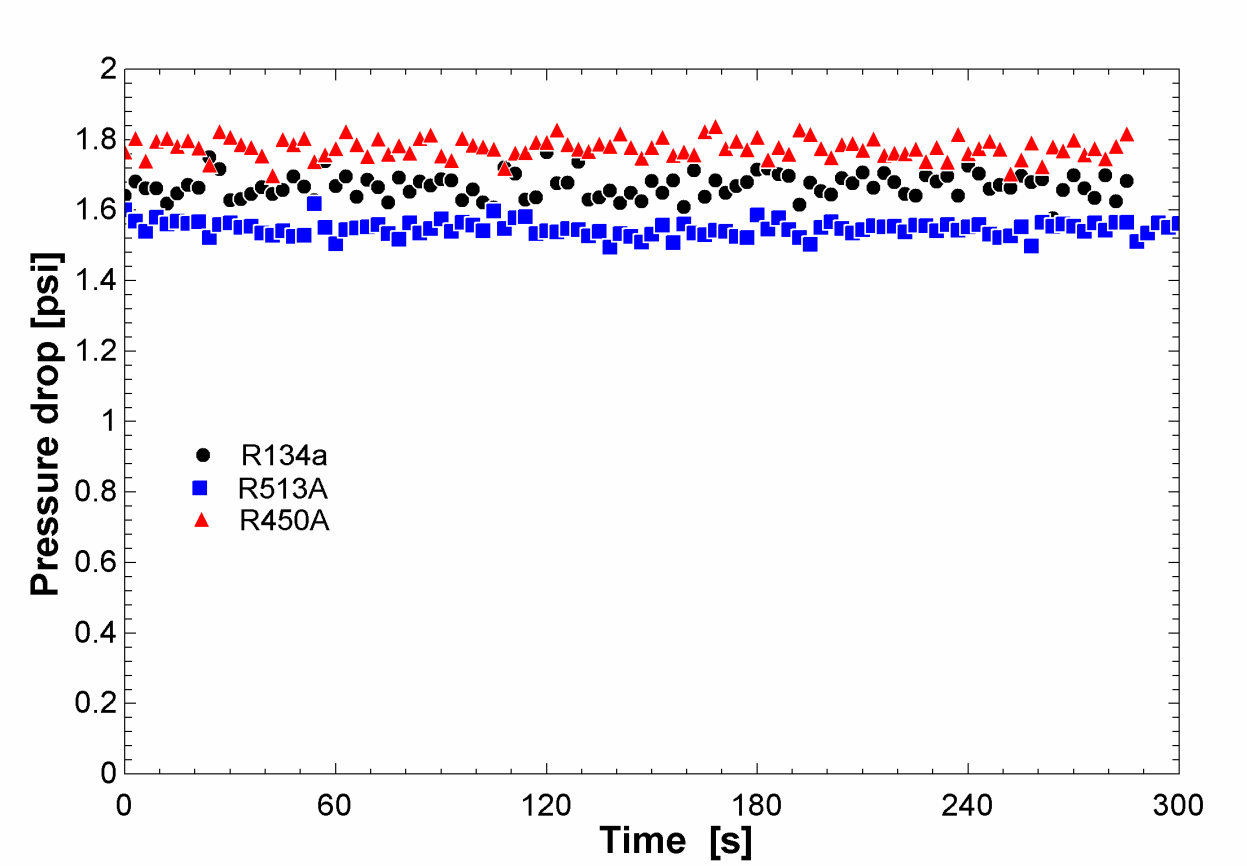

Figure 4.13 Variance in pressure drop with respect to time for R134a, R513A, and R450A at a mass flux of 350 kg/m^{2}s and a quality of 0.5

As with the comparison done for heat transfer coefficients, a second-degree polynomial curve fit equation was calculated from the R134a pressure drop data. The R^2 values for the R134a pressure drop curves are 0.941 (G=200 kg/m^{2}s), 0.862 (G=350 kg/m^{2}s), and 0.996 (G=500 kg/m^{2}s). The equation was used to compare the pressure drops of R513A and R450A to R134a pressure drops. Figure 4.13 presented the comparisons between both R513A and R450A for all three mass fluxes. At a mass flux of 200 kg/m^{2}s, R513A pressure drops were on average 5.2% lower (4.5 – 6.1%) than R134a while R450A pressure drops were on average 3.0% higher (2.5 – 3.7%) than R134a. For a mass flux of 350 kg/m^{2}s, R513A pressure drops were on average 12.9% lower than R134a with minimal variation (i.e., 11.5 – 14.0%); R450A pressure drops averaged

1.8% lower than R134a, but the pressure drops ranged between 6.5% lower than R134a at a quality of 0.25 and 2.1% higher at a quality of 0.87. For a mass flux of 500 kg/m^{2}s, R513A pressure drops were on average 10.5% lower (8.6 – 12.3%) than R134a pressure drops. R450A pressure drops were on average 0.2% lower than R134a pressure drops; however, the pressure drop differences ranged from 9.5% lower at a quality of 0.28 to 5.0% higher at a quality of 0.82. R513A pressure drops are much less effected by quality than R450A which shows lower pressure drop than R134a at low quality, but higher pressure drop at high quality. This is likely due to the R1234ze(E) component of R450A, which has been shown to have higher pressure drop than R134a at high mass flux and quality [141]. R1234ze(E) and R450A do have lower vapor densities than R134a, leading to higher vapor velocities. The higher velocities cause higher pressure drops for R450A than R134a. At 40°C, the vapor density of R134a is 50.09 kg/m^3 and the vapor density of R450A is 50.17 kg/m^3. The lower pressure drop of R513A is likely due to the R1234yf component of R513A, which has been shown to have lower condensation pressure drop than R134a [142]. The vapor densities of R1234yf and R513A are higher than R134a, leading to lower vapor velocities. The lower velocities cause lower pressure drops for R513A than R134a. The vapor density of R513A at 40°C is 54.20 kg/m^3. At one gram per second mass flow rate with a quality of 0.5, the vapor velocities are 9.98 m/s, 8.67 m/s, and 11.13 m/s for R134a, R513A, and R450A, respectively. At three grams per second with a quality of 0.5, the vapor velocities are 29.93 m/s, 26.01 m/s, and 33.39 m/s for R134a, R513A, and R450A, respectively. That is a 13% reduction in vapor velocity for R513A compared to R134a and a 11.5% increase in vapor velocity for R450A compared to R134a.

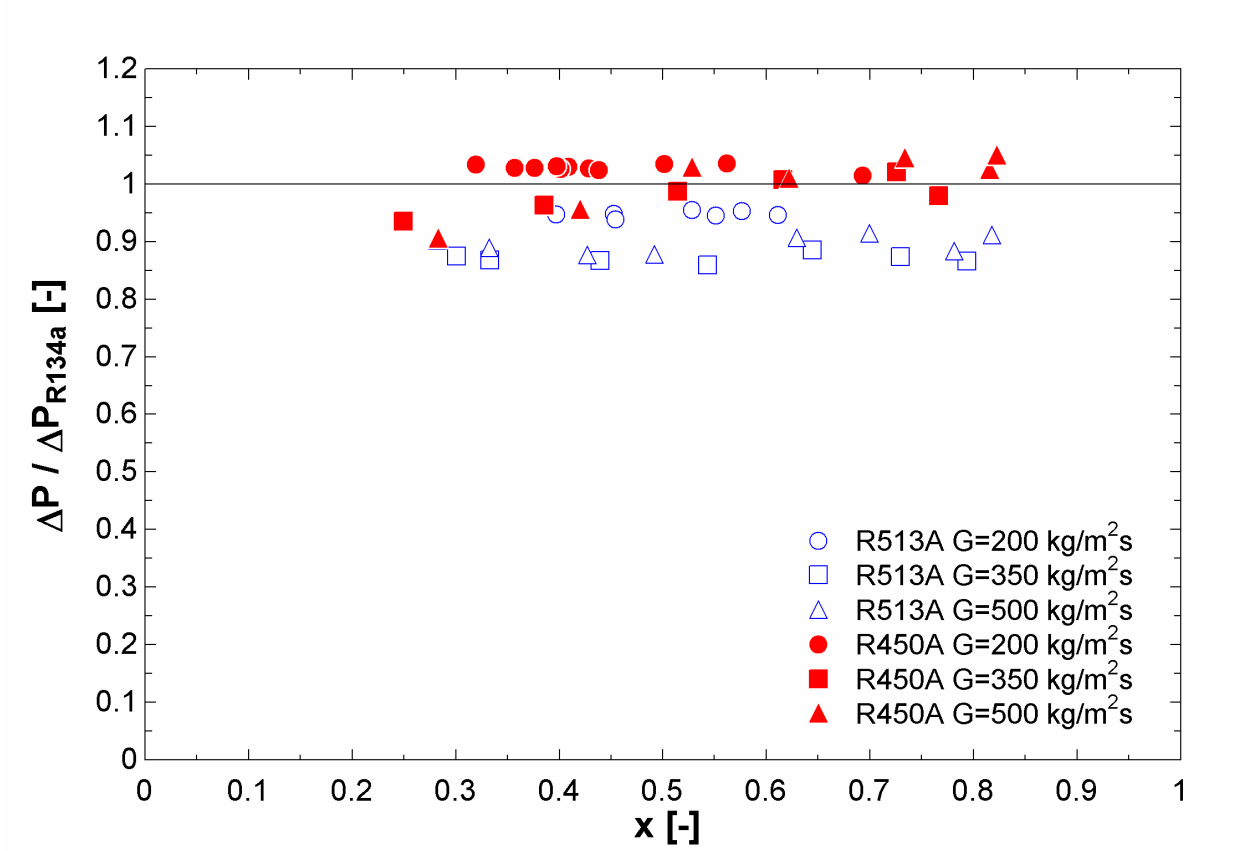

Figure 4.14 Comparison of R513A and R450A to R134a pressure drop for mass fluxes of 200, 350, and 500 kg/m^{2}s

Chapter 5 - Low GWP correlation for flow condensation heat transfer

A new correlation was developed from the low global warming potential refrigerant condensation heat transfer coefficient database developed by the author [8]. The correlation was developed from 11 synthetic refrigerants with GWP lower than 750—R32, R41, R152a, R161, R450A, R452B, R454C, R455A, R513A, R1234yf, and R1234ze(E). The database includes 4,110 data points to be used to develop the correlation. The correlation was developed with 80% of the data points, with 20% set aside to use for testing the correlation.

The correlation was developed using the Buckingham Pi theorem. First, the important parameters in determining the heat transfer coefficients were identified. These include mass flux, quality, temperature, tube diameter, and refrigerant liquid properties including density, viscosity, thermal conductivity, latent heat of vaporization, specific heat, and surface tension. Surface tension was included because systems are using more mini- and micro-channel tubes to increase performance and reduce refrigerant charge and the greater influence of surface tension in smaller diameter tubes. Much of the data (i.e., 61%) were collected in tube diameters less than 3 mm. All fluid properties were liquid phase properties since the liquid film resistance is the largest determiner of condensation performance. Based on the selected parameters, there were four dimensions in the system (i.e., mass, length, time, and temperature). With 11 parameters and 4 dimensions, there were 7 Pi groups. Next, the four important repeating parameters were selected as tube diameter, liquid viscosity, liquid density, and liquid thermal conductivity. These four were selected because of previous knowledge of important non-dimensional numbers used in condensation heat transfer and an understanding of important parameters in condensation heat

transfer; they are also independent of each other. With the four important parameters selected, the seven Pi groups were developed in the form

$$\Pi_i = \alpha \rho_l^a \mu_l^b k_l^c D^d, i = 1, \dots, 7 \tag{5.1}$$

where Π_i is the corresponding Pi group, α is the corresponding non-repeating parameter, and a, b, c, and d are the coefficients to be calculated for each Pi group. After calculating the coefficients for each Pi group, the seven Pi groups are as follows:

$$\Pi_1 = h k_l^{-1} D \tag{5.2}$$

$$\Pi_2 = \sigma \rho_l \mu_l^{-2} D \tag{5.3}$$

$$\Pi_3 = i_{lv} \rho_l^2 \mu_l^{-2} D^2 \tag{5.4}$$

$$\Pi_4 = c_{p,l} \mu_l k_l^{-1} \tag{5.5}$$

$$\Pi_5 = G \mu_l^{-1} D \tag{5.6}$$

$$\Pi_6 = T_{abs} \rho_l^2 \mu_l^{-3} k_l D^2 \tag{5.7}$$

$$\Pi_7 = x \tag{5.8}$$

Based on the Buckingham Pi Theorem, the correlation of the first Pi group is a product of the other Pi groups.

$$\Pi_1 = A \Pi_2^a \Pi_3^b \Pi_4^c \Pi_5^d \Pi_6^e \Pi_7^f \tag{5.9}$$

There are several well-known non-dimensional numbers in this group; Π_1 is the Nusselt number, Π_2 is the liquid Suratmann number, Π_4 is the liquid Prandtl number, and Π_5 is the liquid Reynolds number. Given these non-dimensional numbers and rearranging, the correlation is of the form:

$$Nu = A Re_{lo}^a Pr_l^b Su_{lo}^c x^d \Pi_3^e \Pi_6^f \tag{5.10}$$

With the form of the correlation developed, the next question was if one equation is sufficient or if breaking it into multiple equations is a better choice. Considering the range of data, two viable options were considered – the physical criteria (i.e., tube diameter) and the flow regime

criteria. To incorporate the physics of condensation into the correlation, the flow regime criteria seemed the better option since the data cover both macro- and mini-channel tube diameters. Other well-known correlations have successfully used flow regime criteria [109, 124, 125, 130, 132-134]. Based on the importance of mini-channels for low GWP refrigerants, the correlation was split between two flow regimes – annular flow and non-annular flow – similar to Kim and Mudawar [133]. However, the criteria for annular flow was selected from the analysis done by Nema et al. [104]. The criteria are as follows:

For $Bo \leq Bo_{crit}$, annular flow occurs for $We_v \geq 35$ or $We_v < 35$ and $X_{tt} \leq 0.3521$

For $Bo > Bo_{crit}$, annular flow occurs for $We_v > [6+7(Bo-Bo_{crit})^{1.5}]$

The Bond (Bo) number is compared to a critical Bond number, which represents the relative importance of gravity and surface tension when the minimum liquid volume is present for a slug to develop at the transition point of annular to intermittent flow [104]. When the Bond number, which is a ratio of gravitational forces over surface tension forces, is less than the critical Bond number, it represents smaller diameter tubes where gravity has less effect on flow. In this situation, the transition to annular flow is well documented and determined using the vapor Weber number [101]. As the diameter increases (i.e., Bond number greater than the critical Bond number), gravity has a greater impact and the transition to annular flow is less clear. The vapor Weber number transition coefficient and exponent were determined by regression [104]. The definitions of each non-dimensional number can be found in Table 5.1.

Once the form of the correlation as developed, the MATLAB Optimization toolbox was used to optimize the equations using the 80% test data. The program optimizes the coefficients of the correlations using a non-linear least squares method. The initial guess values were varied to

ensure solution was the global minimum, and not a local minimum. Running the program, the data produced the following correlation:

Annular flow regime:

$$Nu = 0.0547 Re_{lo}^{0.6048} Pr_l^{0.6493} Su_{lo}^{0.5896} x^{0.4729} \Pi_3^{0.0863} \Pi_6^{-0.2696} \quad (5.11)$$

Non-annular flow regime:

$$Nu = 0.0511 Re_{lo}^{0.5165} Pr_l^{-0.0665} Su_{lo}^{-0.3697} x^{0.4188} \Pi_3^{1.1328} \Pi_6^{-0.8537} \quad (5.12)$$

Table 5.1 presents the new correlation with the transition criteria.

Table 5.1 New correlation presented with transition criteria and important parameters

Annular flow:
For $Bo \leq Bo_{crit}$, $We_v \geq 35$ or $We_v < 35$ and $X_{tt} \leq 0.3521$ For $Bo > Bo_{crit}$, $We_v > [6+7(Bo-Bo_{crit})^{1.5}]$
$Nu = 0.0547 Re_{lo}^{0.6048} Pr_l^{0.6493} Su_{lo}^{0.5896} x^{0.4729} \Pi_3^{0.0863} \Pi_6^{-0.2696}$
Non-annular flow:
For $Bo \leq Bo_{crit}$, $We_v \leq 35$ or $We_v > 35$ and $X_{tt} \geq 0.3521$ For $Bo > Bo_{crit}$, $We_v < [6+7(Bo-Bo_{crit})^{1.5}]$
$Nu = 0.0511 Re_{lo}^{0.5165} Pr_l^{-0.0665} Su_{lo}^{-0.3697} x^{0.4188} \Pi_3^{1.1328} \Pi_6^{-0.8537}$
Important parameters:
$Bo = \frac{(\rho_l - \rho_v) g D^2}{\sigma}$ $Bo_{crit} = \frac{1}{\left(\frac{\rho_l}{\rho_l - \rho_v} - \frac{\pi}{4}\right)}$ $We_v = \frac{G^2 D}{\rho_v \sigma}$ $X_{tt} = \left(\frac{\mu_l}{\mu_v}\right)^{0.1} \left(\frac{1-x}{x}\right)^{0.9} \left(\frac{\rho_v}{\rho_l}\right)^{0.5}$ $Nu = \frac{h k_l}{D}$ $Re_{lo} = \frac{GD}{\mu_l}$ $Pr_l = \frac{\mu_l c_{p,l}}{k_l}$

$$Su_{lo} = \frac{\rho_l \sigma D}{\mu_l^2}$$

$$\Pi_3 = \frac{i_{lv} \rho_l^2 D^2}{\mu_l^2}$$

$$\Pi_6 = \frac{T_{abs} \rho_l^2 k_l D^2}{\mu_l^3}$$

Analysis of the correlation gives a build MAE of 24.2%. The correlations for the two flow regimes show that the MAE for annular flow is 25.4% and the MAE for non-annular flow is 21.3%. The developed correlation was tested against the 20% of data held for testing. The MAE for the test data group was 24.6%, which shows consistency in the correlation. The proposed correlation predicted 425 out of 821 (i.e., 51.8%) of the test data points within 20% and 726 out of 821 (i.e., 88.4%) within 50%. The correlation predictions are comparable to the correlations investigated by the author [8], where the best prediction was 26% for Shah [132]. Table 5.2 presents the parameter ranges from the database used to develop the correlation

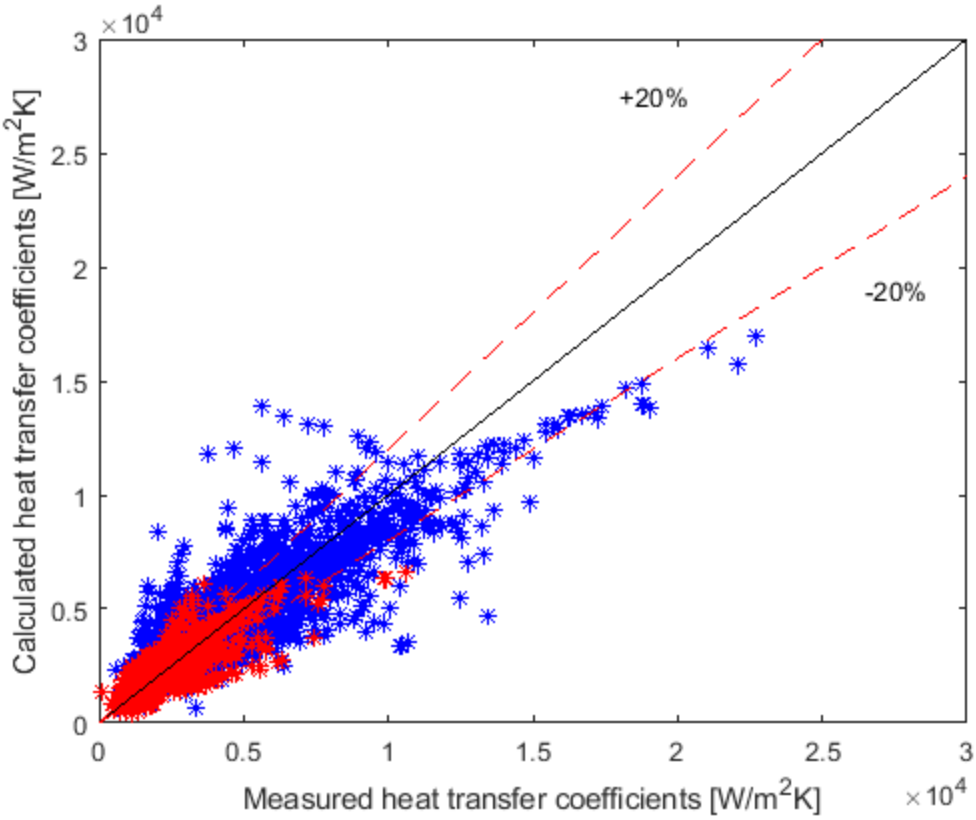

Figure 5.1 Experimental heat transfer coefficients versus heat transfer coefficients calculated from data used to build new correlation where blue data points are annular flow and red data points are non-annular flow

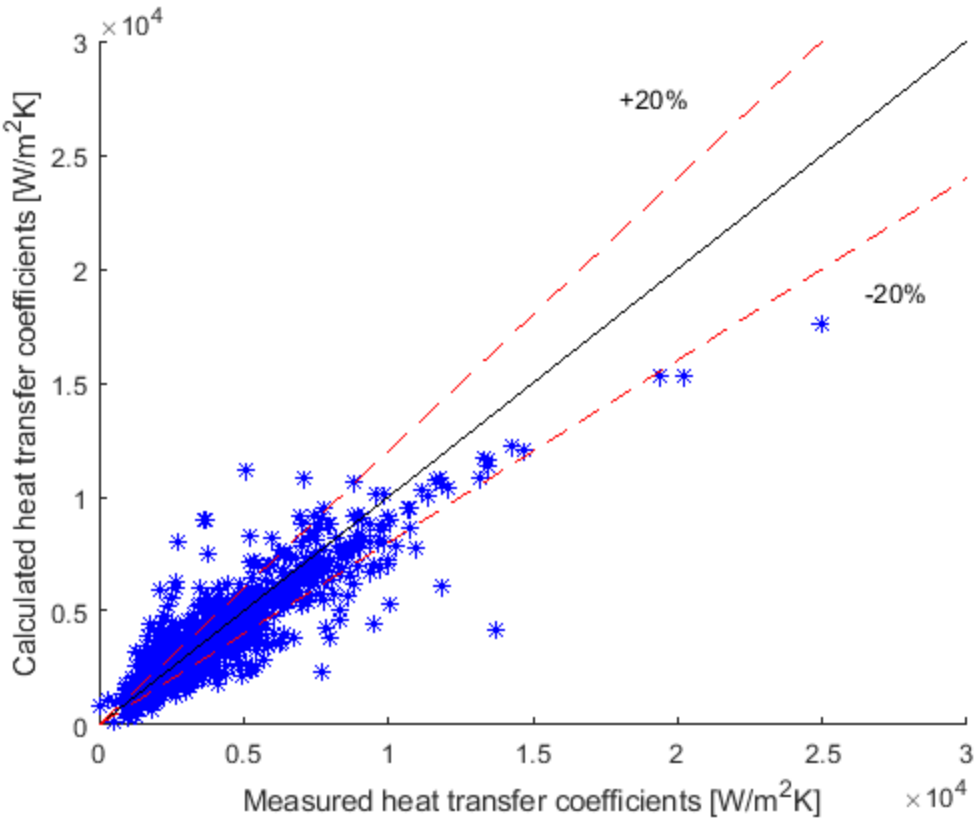

Figure 5.2 Experimental heat transfer coefficients versus heat transfer coefficients predicted by new correlation using data set aside for correlation testing

Table 5.2 Parameter ranges from database used for developing and testing condensation correlation

Parameter [Units]	Range
Refrigerants	R32, R41, R152a, R161, R450A, R452B, R454C, R455A, R513A, R1234yf, R1234ze(E)
Data points	4110
Diameter [mm]	0.5 – 12.7
Saturation Temperature [°C]	15 – 83
Mass flux [kg/m^{2}s]	50 – 1200
Quality [-]	0.007 – 0.999
Liquid density [kg/m^3]	456.5 – 1146
Liquid viscosity [μPa s]	46.7 – 178.4
Liquid thermal conductivity [mW/m K]	52.19 – 118.5
Surface tension [mN/m]	0.2298 – 9.045
Latent heat of vaporization [kJ/kg]	104.4 – 321.6
Specific heat [J/kg K]	1347 – 11482
Pressure ratio [-]	0.15 – 0.91

Liquid Reynolds number	347 – 80084
Liquid Prandtl number	1.87 – 5.64
Liquid Suratmann number	96368 – 4482085
PI3	1.96E12 – 2.64E15
PI6	1.80E12 – 4.28E15
Vapor Weber number	8.35 – 27334
Bond number	0.454 – 616

Chapter 6 - Conclusions and future work

A vapor compression cycle was built to measure flow condensation heat transfer coefficients of R134a and its lower global warming potential alternatives R513A and R450A. Condensation heat transfer coefficients were presented at a diameter of 0.95 mm, mass flux range of 200 – 500 kg/m^{2}s, qualities between 0.2 – 0.8, and a saturation temperature of 40°C. Using the new experimental data and a low global warming potential condensation heat transfer coefficient database the author developed [8], the Buckingham Pi theorem was used to develop a new condensation heat transfer coefficient correlation for synthetic refrigerants with global warming potential less than 750. The major conclusions from this study are:

- R513A heat transfer coefficients were on average 14.8% lower than R134a heat transfer coefficients for all mass fluxes and qualities, ranging from 2.6% to 25.6% lower. At low mass flux (i.e., 200 kg/m^{2}s), the differences were consistently between 13.9% and 18.7% across the quality range (i.e., 0.40 – 0.61). At a mass flux of 350 kg/m^{2}s, the differences ranged from 10.5 – 25.6% with the smallest difference at high quality (i.e., 0.79) and the larger differences at qualities below 0.6. At the highest mass flux (i.e., 500 kg/m^{2}s), the differences ranged from 2.6 – 16.5% with the smallest difference at the highest quality (i.e., 0.82) and the biggest difference at the lowest quality (i.e., 0.28). R513A heat transfer coefficients showed greater differences at lower mass fluxes and qualities and trended toward performance similar to R134a at high mass flux (i.e., 500 kg/m^{2}s) and quality.
- R450A heat transfer coefficients were on average 5.5% lower than R134a heat transfer coefficients were all mass fluxes and qualities, ranging from 2.4% higher to 11.7% lower than R134a. At a mass flux of 200 kg/m^{2}s, the differences ranged between 1.4 – 11.7% lower than R134a with the smallest difference at the highest quality (i.e., 0.69). At a mass

flux of 350 kg/m^{2}s, the differences ranged between 2.4 – 8.7% lower than R134a. At the highest mass flux (i.e., 500 kg/m^{2}s), the differences ranged between 8.8% lower to 2.4% higher than R134a. The biggest lower difference was at the lowest quality (i.e., 0.28), and the biggest higher difference was at the highest quality (i.e., 0.82).

- Three existing correlations were compared to the new experimental data and predicted the data fairly well. Kim and Mudawar [133] had a mean average error of 18.7%, while Shah [132] and Cavallini et al. [129] had a mean average error of 26.2%. All correlations predicted R134a the best, followed by R513A then R450A. The temperature glide of R450A likely contributed to the larger errors.
- A new correlation was developed for low global warming potential synthetic refrigerants with GWP values less than 750. The correlation was developed using 80% of the condensation heat transfer coefficient database including the new experimental data for R513A and R450A. The new correlation was then tested against the other 20% of the database. The mean average error of the data points used to build the correlation was 24.2% and the mean average error of the data points used to test the correlation was 24.6%. The minor differences in mean average error between the two data sets shows consistency in the ability of the correlation to predict these fluids. The mean average errors of the new correlation are comparable to the best correlations that were tested against the database used to develop this correlation from the author's previous work [8].

There is potential for future work in a couple directions from this project. One potential direction includes continuing to grow the condensation heat transfer database as more data is published for new low global warming potential refrigerants. Growing the database allows for continual testing and improving of the correlations to best predict condensation heat transfer

coefficient data for low GWP refrigerants. The second potential direction is to investigate how to modify the apparatus to be able to test multiple hydraulic diameters or channel shapes, expand the quality ranges and mass fluxes where data can be collected, and to reduce uncertainties, especially when the differences in performance of these refrigerants can be 10% or less. The apparatus could also be modified to be able to study flammable refrigerants safely. The third potential direction is to collect condensation heat transfer coefficient data on new refrigerant mixtures that could be potential replacements for current refrigerants, thereby also continuing to expand the database of fundamental condensation heat transfer coefficients of low GWP refrigerants.

Nomenclature

A	area, m
A_s	surface area, m
c_p	specific heat, J/kg K
D	diameter, m
$\frac{dT}{dy}$	temperature gradient in the y direction, K/m
g	gravity, m/s^2
G	mass flux, kg/m^2s
h	heat transfer coefficient, W/m^2K
i_{lv}	latent heat of vaporization, J/kg
I	enthalpy, J/kg
K	thermal conductivity, W/m K
$\dot{m}$	mass flow rate, kg/s
q''	heat flux, W/m^2
$\dot{Q}$	heat transfer, W
T	temperature, °C
x	quality
y	distance in the vertical direction, m
Non-dimensional numbers:	
Bo	Bond number
Nu	Nusselt number
Pr	Prandtl number
Re	Reynolds number
Su	Suratmann number
We	Weber number
X	Lockhart-Martinelli parameter
Greek:	
Φ	two-phase multiplier
μ	viscosity, Pa s

Π	Buckingham Pi group
ρ	density, kg/m^3
σ	surface tension, N/m
ω	uncertainty
Subscripts:	
A, B, C	pertaining to location A, B, C
abs	absolute
block	pertaining to the heat flux block
ch	channel
crit	critical
cu	copper
fluid	pertaining to the fluid
header	pertaining to the header
in	inlet
l	liquid
lo	liquid only
out	outlet
pre	precondenser
ref	refrigerant
tc	thermocouple
tt	turbulent-turbulent
v	vapor
vo	vapor only
wall	pertaining to the wall
water	pertaining to water

References

1. Calm, J.M., *The next generation of refrigerants–Historical review, considerations, and outlook.* International Journal of Refrigeration, 2008. **31**(7): p. 1123-1133.
2. Cavallini, A., D. Del Col, and L. Rossetto, *Heat transfer and pressure drop of natural refrigerants in minichannels (low charge equipment).* International Journal of Refrigeration, 2013. **36**(2): p. 287-300.
3. Yan, Y.-Y. and T.-F. Lin, *Condensation heat transfer and pressure drop of refrigerant R-134a in a small pipe.* International Journal of Heat and Mass Transfer, 1999. **42**(4): p. 697-708.
4. Shah, R.K., *Automotive air-conditioning systems—Historical developments, the state of technology, and future trends.* Heat Transfer Engineering, 2009. **30**(9): p. 720-735.
5. Sethi, A., E.V. Becerra, and S.Y. Motta, *Low GWP R134a replacements for small refrigeration (plug-in) applications.* International Journal of Refrigeration, 2016. **66**: p. 64-72.
6. Bolaji, B. and Z. Huan, *Ozone depletion and global warming: Case for the use of natural refrigerant–a review.* Renewable and Sustainable Energy Reviews, 2013. **18**: p. 49-54.
7. Miyara, A., *Condensation of hydrocarbons–A review.* International Journal of Refrigeration, 2008. **31**(4): p. 621-632.
8. Morrow, J.A., et al., *Flow condensation heat transfer performance of natural and emerging synthetic refrigerants.* International Journal of Refrigeration, 2021.
9. Reddy, D.R., P. Bhramara, and K. Govindarajulu, *Hydrocarbon Refrigerant mixtures as an alternative to R134a in Domestic Refrigeration system: The state-of-the-art review.* International Journal of Scientific & Engineering Research, 2016. **7**(6): p. 87.
10. Harby, K., *Hydrocarbons and their mixtures as alternatives to environmental unfriendly halogenated refrigerants: An updated overview.* Renewable and Sustainable Energy Reviews, 2017. **73**: p. 1247-1264.
11. BABU, P.S., *Ternary mixtures as long term alternative refrigerants for R12 and R134a–a review.* Int. J. Res. Eng. Technol., 2015. **3**(5): p. 9-16.
12. Nawaz, K., et al., *R290 (propane) and R600a (isobutane) as natural refrigerants for residential heat pump water heaters.* Applied Thermal Engineering, 2017. **127**: p. 870-883.
13. Dhavale, S. and D.M. Deshmukh, *Performance Comparison of Hydrocarbon Refrigerant as Isobutane R600a and Propane R290 in Domestic Refrigerator as Alternative Refrigerants to R134a.* Invention Journal of Research Technology in Engineering & Management (IJRTEM), 2016. **1**: p. 2455-3689.
14. Bellos, E. and C. Tzivanidis, *Investigation of the environmentally-friendly refrigerant R152a for air conditioning purposes.* Applied Sciences, 2019. **9**(1): p. 119.
15. Cabello, R., et al., *Experimental comparison between R152a and R134a working in a refrigeration facility equipped with a hermetic compressor.* international journal of refrigeration, 2015. **60**: p. 92-105.
16. Nie, J., et al., *Analysis and comparison study on different HFC refrigerants for space heating air source heat pump in rural residential buildings of north China.* Procedia Engineering, 2017. **205**: p. 1201-1206.

17. Sánchez, D., et al., *Energy performance evaluation of R1234yf, R1234ze (E), R600a, R290 and R152a as low-GWP R134a alternatives.* International Journal of Refrigeration, 2017. **74**: p. 269-282.
18. Bolaji, B., *Experimental study of R152a and R32 to replace R134a in a domestic refrigerator.* Energy, 2010. **35**(9): p. 3793-3798.
19. Yang, W.-w., et al., *Theoretical study of a high-temperature heat pump system composed of a CO2 transcritical heat pump cycle and a R152a subcritical heat pump cycle.* Applied thermal engineering, 2017. **120**: p. 228-238.
20. Cabello, R., et al., *Energy evaluation of R152a as drop in replacement for R134a in cascade refrigeration plants.* Applied Thermal Engineering, 2017. **110**: p. 972-984.
21. Pérez-García, V., et al., *Second law analysis of a mobile air conditioning system with internal heat exchanger using low GWP refrigerants.* Entropy, 2017. **19**(4): p. 175.
22. Righetti, G., et al., *A review on in-tube two-phase heat transfer of hydro-fluoro-olefines refrigerants.* Science and Technology for the Built Environment, 2016. **22**(8): p. 1191-1225.
23. Nair, V., *HFO refrigerants: A review of present status and future prospects.* International Journal of Refrigeration, 2021.
24. Longo, G.A., et al., *Assessment of the low-GWP refrigerants R600a, R1234ze (Z) and R1233zd (E) for heat pump and organic Rankine cycle applications.* Applied Thermal Engineering, 2020. **167**: p. 114804.
25. Fukuda, S., et al., *Low GWP refrigerants R1234ze (E) and R1234ze (Z) for high temperature heat pumps.* International journal of Refrigeration, 2014. **40**: p. 161-173.
26. Nagata, R., C. Kondou, and S. Koyama, *Comparative assessment of condensation and pool boiling heat transfer on horizontal plain single tubes for R1234ze (E), R1234ze (Z), and R1233zd (E).* International Journal of Refrigeration, 2016. **63**: p. 157-170.
27. Brown, J.S., et al., *Thermophysical properties and heat transfer and pressure drop performance potentials of hydrofluoro-olefins, hydrochlorofluoro-olefins, and their blends.* HVAC&R Research, 2014. **20**(2): p. 203-220.
28. Eyerer, S., et al., *Experimental study of an ORC (Organic Rankine Cycle) and analysis of R1233zd-E as a drop-in replacement for R245fa for low temperature heat utilization.* Energy, 2016. **103**: p. 660-671.
29. Huang, H., N. Borhani, and J.R. Thome, *Experimental investigation on flow boiling pressure drop and heat transfer of R1233zd (E) in a multi-microchannel evaporator.* International Journal of Heat and Mass Transfer, 2016. **98**: p. 596-610.
30. Yang, Z., et al., *Experimental measurement and modelling of vapor-liquid equilibrium for 3, 3, 3-Trifluoropropene (R1243zf) and trans-1, 3, 3, 3-Tetrafluoropropene (R1234ze (E)) binary system.* International Journal of Refrigeration, 2020. **120**: p. 137-149.
31. Mota-Babiloni, A., et al., *A review of refrigerant R1234ze (E) recent investigations.* Applied Thermal Engineering, 2016. **95**: p. 211-222.
32. Agarwal, R. and P. Hrnjak, *Condensation in two phase and desuperheating zone for R1234ze (E), R134a and R32 in horizontal smooth tubes.* International Journal of Refrigeration, 2015. **50**: p. 172-183.
33. Pabon, J.J., et al., *Applications of refrigerant R1234yf in heating, air conditioning and refrigeration systems: A decade of researches.* International Journal of Refrigeration, 2020. **118**: p. 104-113.

34. Heredia-Aricapa, Y., et al., *Overview of low GWP mixtures for the replacement of HFC refrigerants: R134a, R404A and R410A.* International Journal of Refrigeration, 2020. **111**: p. 113-123.
35. Poongavanam, G., et al., *Selection of the best refrigerant for replacing R134a in automobile air conditioning system using different MCDM methods: A comparative study.* Case Studies in Thermal Engineering, 2021. **27**: p. 101344.
36. Abraham, J.A.P. and M. Mohanraj, *Thermodynamic performance of automobile air conditioners working with R430A as a drop-in substitute to R134a.* Journal of Thermal Analysis and Calorimetry, 2019. **136**(5): p. 2071-2086.
37. Mohanraj, M., *Energy performance assessment of R430A as a possible alternative refrigerant to R134a in domestic refrigerators.* Energy for sustainable development, 2013. **17**(5): p. 471-476.
38. Bolaji, B.O., et al., *Theoretical investigation of energy-saving potential of eco-friendly R430A, R440A and R450A refrigerants in a domestic refrigerator.* Iranian Journal of Science and Technology, Transactions of Mechanical Engineering, 2019. **43**(1): p. 103-112.
39. Park, K.-J. and D. Jung, *Performance of alternative refrigerant R430A on domestic water purifiers.* Energy conversion and management, 2009. **50**(12): p. 3045-3050.
40. Shodiya, S., M. Oumarou, and A. Abdulrahim, *Assessment of R430A refrigerant as a possible substitute to R134a refrigerant in large capacity freezer.* ASSESSMENT, 2015. **6**.
41. Alihosseini, N., G. Salehi, and A.M. Lavasani, *Exergy and exergoeconomic analyses of serial and bypass two-stage compression on the household refrigerator-freezer and replacement of R436A refrigerant.* Proceedings of the Institution of Mechanical Engineers, Part A: Journal of Power and Energy, 2021: p. 09576509211032495.
42. Hastak, S.S. and J.M. Kshirsagar. *Comparative performance analysis of R600a and R436a as an alternative of R134a refrigerant in a domestic refrigerator*. in *IOP Conference Series: Materials Science and Engineering*. 2018. IOP Publishing.
43. Rasti, M., et al. *Feasibility of using hydrocarbon mixture (R436a) as refrigerant in domestic refrigerators*. in *13th Iranian National Chemical Engineering Congress & 1st International Regional Chemical and Petroleum Engineering Kermanshah, Iran*. 2010.
44. Rasti, M., S. Aghamiri, and M.-S. Hatamipour, *Energy efficiency enhancement of a domestic refrigerator using R436A and R600a as alternative refrigerants to R134a.* International Journal of Thermal Sciences, 2013. **74**: p. 86-94.
45. Reddy, M.V., C.C. Sekhar, and D.R. Reddy, *Performance Prediction of Domestic Refrigeration System using R436A Refrigerant as alternative Refrigerant to R134a with ANN.* International Journal of Innovative Research in Science, Engineering and Technology, 2017. **6**: p. 19008-19017.
46. Reddy, D.R., P. Bhramara, and K. Govindarajulu, *Experimental evaluation of the effect of refrigerant charge and capillary tube length on the performance of household refrigerator with different configurations of R290 and R600a.* Materials Today: Proceedings, 2018. **5**(5): p. 11845-11852.
47. Rasti, M., et al., *Enhancement of domestic refrigerator's energy efficiency index using a hydrocarbon mixture refrigerant.* Measurement, 2012. **45**(7): p. 1807-1813.

48. Bolaji, B.O., *Theoretical assessment of new low global warming potential refrigerant mixtures as eco-friendly alternatives in domestic refrigeration systems.* Scientific African, 2020. **10**: p. e00632.
49. Prabha, C. and P.K. Mathews, *Exergy Analysis of a Domestic Refrigerator Using Eco-Friendly R441A Refrigerant Mixture as an Alternative to R134A.* International Journal of Applied Engineering Research, 2014. **9**(22): p. 15773-15781.
50. Prabha, C., P.K. Mathews, and S. Arunkumar, *Performance Assessment of an Eco–Friendly Alternate Refrigerant R441a.* International Journal for Research in Emerging Science and Technology. **1**.
51. Back, I. and L. Dunberger, *Evaluating alternative refrigerants for the room air conditioner market.* 2015.
52. Tare, S., S. Purkar, and R. Shukla, *INTERNATIONAL JOURNAL OF ENGINEERING SCIENCES & RESEARCH TECHNOLOGY COMPARATIVE STUDY OF EXERGY LOSS OF REFRIGERANTS DURING CONDENSATION PROCESS OF VCR CYCLE.*
53. Al-Sayyab, A.K.S., J. Navarro-Esbrí, and A. Mota-Babiloni, *Energy, exergy, and environmental (3E) analysis of a compound ejector-heat pump with low GWP refrigerants for simultaneous data center cooling and district heating.* International Journal of Refrigeration, 2021.
54. Direk, M., et al., *Experimental Investigation of an Automotive Air Conditioning System Using R444A and R152a Refrigerants as Alternatives of R134a.* Strojniski Vestnik-Journal of Mechanical Engineering, 2019. **65**(4): p. 212-219.
55. Direk, M. and F. YÜKSEL, *Comparative experimental evaluation on heating performance of a mobile air conditioning system using R134a, R1234ze (E), R152a and R444a.* Isı Bilimi ve Tekniği Dergisi, 2019. **39**(1): p. 31-38.
56. Devecioğlu, A.G. and V. Oruç, *An analysis on the comparison of low-GWP refrigerants to alternatively use in mobile air-conditioning systems.* Thermal Science and Engineering Progress, 2017. **1**: p. 1-5.
57. Colombo, L.P.M., A. Lucchini, and L. Molinaroli, *Analisi sperimentale della sostituzione del R134a con R1234yf, R1234ze (E), R450A e R513A in una pompa di calore acqua-acqua di piccola taglia.* 2019.
58. Makhnatch, P., et al., *R450A and R513A as lower GWP mixtures for high ambient temperature countries: Experimental comparison with R134a.* Energy, 2019. **166**: p. 223-235.
59. Costa, M.S., *Avaliação do uso de r513a no sistema de refrigeração cascata subcrítico.* 2017.
60. Diani, A., P. Brunello, and L. Rossetto, *R513A condensation heat transfer inside tubes: Microfin tube vs. smooth tube.* International Journal of Heat and Mass Transfer, 2020. **152**: p. 119472.
61. López-Belchí, A., *Assessment of a mini-channel condenser at high ambient temperatures based on experimental measurements working with R134a, R513A and R1234yf.* Applied Thermal Engineering, 2019. **155**: p. 341-353.
62. Morrow, J.A., J. Booth, and M. Derby, *Comparison of mini-channel condensation heat transfer for R513A and R134a,* in *17th International Refrigeration and Air Conditioning Conference*. 2018: Purdue University.

63. Saadoon, Y.G. and I.M. Aljubury, *EXPERIMENTAL ANALYSIS OF MOBILE AIR CONDITIONING SYSTEM USING R513A AS ALTERNATIVE REFRIGERANTS TO R134A.*
64. Yıldız, A. and R. Yıldırım, *Investigation of using R134a, R1234yf and R513A as refrigerant in a heat pump.* International Journal of Environmental Science and Technology, 2021. **18**(5): p. 1201-1210.
65. Li, G., *Performance evaluation of low global warming potential working fluids as R134a alternatives for two-stage centrifugal chiller applications.* Korean Journal of Chemical Engineering, 2021: p. 1-14.
66. Du, Y., *Investigation of Performance of Low GWP Alternative to R134a in Centrifugal Chiller.* Journal of Engineering Thermophysics, 2021. **30**(1): p. 103-121.
67. Meng, Z., et al., *Refrigerating fluid with a low global warming potential for automotive air conditioning systems in summer.* Thermal Science, 2021(00): p. 45-45.
68. Sjoholm, L. and Y.C. Ma, *A Study of Low GWP Refrigerants for Transport Refrigeration based on Hermetic Scroll Compressors with an Economizer.* 2018.
69. Schultz, K. and S. Kujak, *System drop-in tests of R134a alternative refrigerants (ARM-42a, N-13a, N-13b, R-1234ze (E), and OpteonTM XP10) in a 230-RT water-cooled water chiller.* Air-Conditioning, Heating, and Refrigeration Institute (AHRI) Low-GWP Alternative Refrigerants Evaluation Program (Low-GWP AREP),(Ed.), 2013.
70. Kontomaris, K., J.P. Kauffman, and S. Kulankara, *A Reduced GWP Replacement for HFC-134a in Centrifugal Chillers: XP10 Measured Performance and Projected Climate Impact.* 2012.
71. Sun, J., W. Li, and B. Cui, *Energy and exergy analyses of R513a as a R134a drop-in replacement in a vapor compression refrigeration system.* International Journal of Refrigeration, 2020. **112**: p. 348-356.
72. Pardo, P. and M. Mondot, *Experimental evaluation of R410A, R407C and R134a alternative refrigerants in residential heat pumps.* 2018.
73. Mota-Babiloni, A., P. Makhnatch, and R. Khodabandeh, *Recent investigations in HFCs substitution with lower GWP synthetic alternatives: Focus on energetic performance and environmental impact.* International Journal of Refrigeration, 2017. **82**: p. 288-301.
74. DEVECİOĞLU, A. and O. Vedat, *A COMPARATIVE ENERGETIC ANALYSIS FOR SOME LOW-GWP REFRIGERANTS AS R134a REPLACEMENTS IN VARIOUS VAPOR.* Isı Bilimi ve Tekniği Dergisi, 2018. **38**(2): p. 51-61.
75. Al-Sayyab, A.K.S., A. Mota-Babiloni, and J. Navarro-Esbrí, *Novel compound waste heat-solar driven ejector-compression heat pump for simultaneous cooling and heating using environmentally friendly refrigerants.* Energy Conversion and Management, 2021. **228**: p. 113703.
76. Belman-Flores, J., et al., *Using ANNs to approach to the energy performance for a small refrigeration system working with R134a and two alternative lower GWP mixtures.* Applied Thermal Engineering, 2017. **127**: p. 996-1004.
77. Yang, Z., et al., *Analysis of lower GWP and flammable alternative refrigerants.* International Journal of Refrigeration, 2021.
78. Llopis, R., et al., *Experimental analysis of R-450A and R-513A as replacements of R-134a and R-507A in a medium temperature commercial refrigeration system.* International journal of refrigeration, 2017. **84**: p. 52-66.

79. Shapiro, D., *Drop-in testing of next-generation R134a alternates in a commercial bottle cooler/freezer.* 2012.
80. Catalán-Gil, J., et al., *Energy evaluation of multiple stage commercial refrigeration architectures adapted to F-gas regulation.* Energies, 2018. **11**(7): p. 1915.
81. Mota-Babiloni, A., et al., *Drop-in analysis of an internal heat exchanger in a vapour compression system using R1234ze (E) and R450A as alternatives for R134a.* Energy, 2015. **90**: p. 1636-1644.
82. Makhnatch, P., A. Mota-Babiloni, and R. Khodabandeh, *Experimental study of R450A drop-in performance in an R134a small capacity refrigeration unit.* International Journal of Refrigeration, 2017. **84**: p. 26-35.
83. Devecioğlu, A.G., V. Oruç, and E. Aras, *COMPARATIVE THERMODYNAMIC ANALYSIS OF R1234YF AND R450A AS SUBSTITUTES FOR R134A IN A VAPOR COMPRESSION REFRIGERATION SYSTEM.* Energy, 2016. **36**: p. 6110-6120.
84. Gatarić, P. and L. Lorbek, *Evaluating R450A as a drop-in replacement for R134a in household heat pump tumble dryers.* International Journal of Refrigeration, 2021. **128**: p. 22-33.
85. Kumaş, K. and A.Ö. AKYÜZ, *Performance Analysis of R450A Refrigerant in Vapor Compression Cooling System for Sustainable Environment.* Akademia Doğa ve İnsan Bilimleri Dergisi, 2020. **6**(1): p. 57-71.
86. John, M., et al. *Potential application of commercial refrigerants as adsorbate in adsorption refrigeration system.* in *ISES Solar World Congress*. 2017.
87. Kandlikar, S.G. and W.J. Grande, *Evolution of microchannel flow passages--thermohydraulic performance and fabrication technology.* Heat transfer engineering, 2003. **24**(1): p. 3-17.
88. Qu, W. and I. Mudawar, *Measurement and correlation of critical heat flux in two-phase micro-channel heat sinks.* International Journal of Heat and Mass Transfer, 2004. **47**(10-11): p. 2045-2059.
89. Agarwal, A. and S. Garimella, *Representative results for condensation measurements at hydraulic diameters∼100 microns.* Journal of Heat Transfer, 2010.
90. Shin, J.S. and M.H. Kim, *An Experimental Study of Flow Condensation Heat Transfer Inside Circular and Rectangular Mini-Channels.* Heat Transfer Engineering, 2005. **26**(3): p. 36-44.
91. Wang, W.-W.W., T.D. Radcliff, and R.N. Christensen, *A condensation heat transfer correlation for millimeter-scale tubing with flow regime transition.* Experimental Thermal and Fluid Science, 2002. **26**(5): p. 473-485.
92. Derby, M., et al., *Condensation heat transfer in square, triangular, and semi-circular mini-channels.* International Journal of Heat and Mass Transfer, 2012. **55**(1-3): p. 187-197.
93. Matkovic, M., et al., *Experimental study on condensation heat transfer inside a single circular minichannel.* International Journal of Heat and Mass Transfer, 2009. **52**(9-10): p. 2311-2323.
94. Cavallini, A., et al., *Condensation in horizontal smooth tubes: a new heat transfer model for heat exchanger design.* Heat Transfer Engineering, 2006. **27**(8): p. 31-38.
95. Diani, A. and L. Rossetto, *Condensation of an Azeotropic Mixture inside 2.5 mm ID Minitubes.* Fluids, 2020. **5**(4): p. 171.

96. Wang, H.S. and J.W. Rose, *Film condensation in horizontal microchannels: Effect of channel shape.* International Journal of Thermal Sciences, 2006. **45**(12): p. 1205-1212.
97. Agarwal, A., T.M. Bandhauer, and S. Garimella, *Measurement and modeling of condensation heat transfer in non-circular microchannels.* International Journal of Refrigeration, 2010. **33**(6): p. 1169-1179.
98. Baker, O. *Design of pipelines for the simultaneous flow of oil and gas*. in *Fall meeting of the petroleum branch of AIME*. 1953. OnePetro.
99. Mandhane, J., G. Gregory, and K. Aziz, *A flow pattern map for gas—liquid flow in horizontal pipes.* International journal of multiphase flow, 1974. **1**(4): p. 537-553.
100. Tandon, T., H. Varma, and C. Gupta, *A new flow regimes map for condensation inside horizontal tubes.* 1982.
101. Coleman, J.W. and S. Garimella, *Two-phase flow regimes in round, square and rectangular tubes during condensation of refrigerant R134a.* International Journal of Refrigeration, 2003. **26**(1): p. 117-128.
102. Garimella, S., *Condensation flow mechanisms in microchannels: basis for pressure drop and heat transfer models.* Heat Transfer Engineering, 2004. **25**.
103. Cavallini, A., et al., *Condensation inside and outside smooth and enhanced tubes—a review of recent research.* International Journal of Refrigeration, 2003. **26**(4): p. 373-392.
104. Nema, G., S. Garimella, and B.M. Fronk, *Flow regime transitions during condensation in microchannels.* International journal of refrigeration, 2014. **40**: p. 227-240.
105. Bohdal, T., H. Charun, and M. Sikora, *Comparative investigations of the condensation of R134a and R404A refrigerants in pipe minichannels.* International Journal of Heat and Mass Transfer, 2011. **54**(9-10): p. 1963-1974.
106. Dobson, M. and J. Chato, *Condensation in smooth horizontal tubes.* 1998.
107. Cavallini, A. and R. Zecchin. *A dimensionless correlation for heat transfer in forced convection condensation*. in *International Heat Transfer Conference Digital Library*. 1974. Begel House Inc.
108. Akers, W., H. Deans, and O. Crosser, *Condensing heat transfer within horizontal tubes.* Chem. Eng. Progr., 1958. **54**.
109. Shah, M.M., *A general correlation for heat transfer during film condensation inside pipes.* International Journal of heat and mass transfer, 1979. **22**(4): p. 547-556.
110. Tang, L., *Empirical study of new refrigerant flow condensation inside horizontal smooth and micro-fin tubes*. 1997: University of Maryland, College Park.
111. Kaew-On, J., et al., *Condensation heat transfer characteristics of R134a flowing inside mini circular and flattened tubes.* International Journal of Heat and Mass Transfer, 2016. **102**: p. 86-97.
112. Sakamatapan, K., et al., *Condensation heat transfer characteristics of R-134a flowing inside the multiport minichannels.* International journal of heat and mass transfer, 2013. **64**: p. 976-985.
113. Del Col, D., et al., *Effect of cross sectional shape during condensation in a single square minichannel.* International journal of heat and mass transfer, 2011. **54**(17-18): p. 3909-3920.
114. Del Col, D., et al. *Minichannel condensation in downward, upward and horizontal configuration*. in *Journal of Physics: Conference Series*. 2012. IOP Publishing.

115. Toninelli, P., et al., *Effects of geometry and fluid properties during condensation in minichannels: experiments and simulations.* Heat and Mass Transfer, 2019. **55**(1): p. 41-57.
116. Goss Jr, G. and J. Passos, *Heat transfer during the condensation of R134a inside eight parallel microchannels.* International Journal of Heat and Mass Transfer, 2013. **59**: p. 9-19.
117. Rahman, M.M., K. Kariya, and A. Miyara, *An experimental study and development of new correlation for condensation heat transfer coefficient of refrigerant inside a multiport minichannel with and without fins.* International Journal of Heat and Mass Transfer, 2018. **116**: p. 50-60.
118. Patel, T., A. Parekh, and P. Tailor, *Experimental analysis of condensation heat transfer and frictional pressure drop in a horizontal circular mini channel.* Heat and Mass Transfer, 2020. **56**(5): p. 1579-1600.
119. Jige, D., N. Inoue, and S. Koyama, *Condensation of refrigerants in a multiport tube with rectangular minichannels.* International Journal of Refrigeration, 2016. **67**: p. 202-213.
120. Karageorgis, A., G. Hinopoulos, and M.-H. Kim, *A Comparative Study on the Condensation Heat Transfer of R-513A as an Alternative to R-134a.* Machines, 2021. **9**(6): p. 114.
121. Jacob, T.A., E.P. Matty, and B.M. Fronk, *Experimental investigation of in-tube condensation of low GWP refrigerant R450A using a fiber optic distributed temperature sensor.* International Journal of Refrigeration, 2019. **103**: p. 274-286.
122. Liu, Y., et al., *Numerical investigation on the condensation of R134a, R1234ze (E) and R450A in mini-channels.* International Journal of Refrigeration, 2021.
123. Thome, J.R., J. El Hajal, and A. Cavallini, *Condensation in horizontal tubes, part 2: new heat transfer model based on flow regimes.* International journal of heat and mass transfer, 2003. **46**(18): p. 3365-3387.
124. Shah, M.M., *An improved and extended general correlation for heat transfer during condensation in plain tubes.* Hvac&R Research, 2009. **15**(5): p. 889-913.
125. Shah, M.M., *General Correlation For Heat Transfer During Condensation in Plain Tubes: Further Development and Verification.* ASHRAE Transactions, 2013. **119**(2).
126. Traviss, D., et al., *FORCED-CONVECTION CONDENSATION INSIDE TUBES: A HEAT TRANSFERT EQUATION FOR CONDENSER DESIGN.* 1973.
127. Jung, D., et al., *Flow condensation heat transfer coefficients of pure refrigerants.* International Journal of Refrigeration, 2003. **26**(1): p. 4-11.
128. Moser, K., R. Webb, and B. Na, *A new equivalent Reynolds number model for condensation in smooth tubes.* 1998.
129. Cavallini, A., et al., *Condensation heat transfer and pressure losses of high-and low-pressure refrigerants flowing in a single circular minichannel.* Heat Transfer Engineering, 2011. **32**(2): p. 90-98.
130. Cavallini, A., et al., *Update on condensation heat transfer and pressure drop inside minichannels.* Heat Transfer Engineering, 2006. **27**(4): p. 74-87.
131. Bandhauer, T.M., A. Agarwal, and S. Garimella, *Measurement and modeling of condensation heat transfer coefficients in circular microchannels.* 2006.
132. Shah, M.M., *A correlation for heat transfer during condensation in horizontal mini/micro channels.* International Journal of Refrigeration, 2016. **64**: p. 187-202.

133. Kim, S.-M. and I. Mudawar, *Universal approach to predicting heat transfer coefficient for condensing mini/micro-channel flow.* International Journal of Heat and Mass Transfer, 2013. **56**(1-2): p. 238-250.
134. Macdonald, M. and S. Garimella, *Hydrocarbon condensation in horizontal smooth tubes: Part II–Heat transfer coefficient and pressure drop modeling.* International Journal of Heat and Mass Transfer, 2016. **93**: p. 1248-1261.
135. Derby, M.M., et al., *Flow condensation heat transfer enhancement in a mini-channel with hydrophobic and hydrophilic patterns.* International Journal of Heat and Mass Transfer, 2014. **68**: p. 151-160.
136. Derby, M.M., *Study of flow condensation enhancement with hydrophobic and hydrophilic patterns*. 2013: Rensselaer Polytechnic Institute.
137. Kline, S.J. and F.A. McClintock, *Describing uncertainty in single sample experiments.* ASME Mech Eng., 1953. **75**: p. 3-8.
138. Kedzierski, M.A. and J.L. Worthington III, *Design and machining of copper specimens with micro holes for accurate heat transfer measurements.* Experimental heat transfer, 1993. **6**(4): p. 329-344.
139. Wibulswas, P., *Laminar-flow heat-transfer in non-circular ducts*. 1966, University of London.
140. Gnielinski, V., *A new method to calculate heat transfer in the transition region between laminar and turbulent tube flow; Ein neues Berechnungsverfahren fuer die Waermeuebertragung im Uebergangsbereich zwischen laminarer und turbulenter Rohrstroemung.* Forschung im Ingenieurwesen, 1995. **61**.
141. Wang, J. and J.M. Li, *Pressure drop of R134a and R1234ze (E) during condensation in horizontal microchannel arrays cooled symmetrically and asymmetrically.* Experimental Thermal and Fluid Science, 2018. **96**: p. 266-283.
142. Illán-Gómez, F., et al., *Experimental two-phase heat transfer coefficient and frictional pressure drop inside mini-channels during condensation with R1234yf and R134a.* International Journal of Refrigeration, 2015. **51**: p. 12-23.

Appendix A - Experimental condensation heat transfer coefficient data

Table A.1 Experimental condensation heat transfer coefficient data for R134a, R513A, and R450A in 0.95 mm diameter channels

Ref	T_{sat} [°C]	T_{wall} [°C]	G [kg/m^{2}s]	x [-]	h [W/m^{2}K]	ω_h [W/m^{2}K]	ΔP [psi]
R134a	39.49	28.44	192.6	0.5959	2941	295.4	1.209
R134a	39.43	27.94	192.6	0.5312	2762	282.8	1.197
R134a	39.24	27.42	192.6	0.4844	2617	273.8	1.183
R134a	39.31	27.06	188.1	0.4167	2477	263.1	1.173
R134a	39.48	26.61	188.1	0.3519	2305	249.7	1.163
R134a	39.75	27.51	345	0.4673	3630	276.2	1.67
R134a	39.97	27.56	340.5	0.4492	3592	272.2	1.668
R134a	40.16	27.67	340.5	0.4459	3594	270.6	1.66
R134a	39.63	27.19	340.5	0.4273	3503	270.4	1.628
R134a	39.71	28.63	358.5	0.6634	4854	321.1	1.984
R134a	40.29	28.36	345	0.5634	4461	294.5	1.924
R134a	40.37	25.72	358.5	0.3221	3165	229	1.591
R134a	40.15	28.64	497.4	0.4567	4640	307	2.443
R134a	39.83	27.4	497.4	0.3587	4035	277.6	2.187
R134a	39.76	26.13	497.4	0.2588	3435	247.8	1.918
R134a	40.12	29.15	497.4	0.5131	4993	326.3	2.575
R134a	40.29	30.02	497.4	0.5889	5550	356.5	2.79
R134a	40.81	31.24	497.4	0.6852	6278	394.3	3.02
R134a	40.08	30.88	488.5	0.7701	6414	411.5	3.093
R134a	39.65	28.71	345	0.706	4938	326.2	1.916
R134a	40.05	24.71	197.1	0.5766	2880	216.4	1.219
R513A	40.08	25.09	201.7	0.6111	2443	216.9	1.156
R513A	39.7	27.43	201.7	0.5764	2425	262.5	1.154
R513A	39.58	26.99	201.7	0.528	2309	254.9	1.143
R513A	39.27	26.9	201.7	0.5513	2329	259.5	1.138

Ref	T_{sat} [°C]	T_{wall} [°C]	G [kg/m^{2}s]	x [-]	h [W/m^{2}K]	ω_h [W/m^{2}K]	ΔP [psi]
R513A	39.17	25.92	201.7	0.4529	2085	241	1.119
R513A	39.63	32.87	201.7	0.454	2208	467.7	1.108
R513A	39.41	28.4	201.7	0.397	1964	287.7	1.108
R513A	39.75	33.6	345.6	0.7937	4888	559.3	1.8
R513A	39.45	32.9	345.6	0.7295	4512	518.2	1.755
R513A	39.34	32.05	345.6	0.6441	3961	457.9	1.693
R513A	40.09	31.41	345.6	0.5429	3250	377	1.546
R513A	40.02	29.75	350.2	0.4392	2697	314.6	1.457
R513A	39.49	28.87	345.6	0.333	2482	302.3	1.352
R513A	39.54	28.36	345.6	0.3005	2332	286.2	1.33
R513A	40.1	35.05	498.7	0.8173	6712	731.3	2.919
R513A	40.39	34.94	489.4	0.781	6230	665	2.778
R513A	39.81	34.07	498.7	0.6993	5769	619.9	2.74
R513A	39.22	33.11	498.7	0.629	5264	571.6	2.591
R513A	40.17	32.41	498.7	0.4916	4180	434.8	2.233
R513A	39.58	31.42	498.7	0.4271	3803	408.3	2.088
R513A	38.79	29.83	498.7	0.3322	3274	365.7	1.887
R513A	39.48	30.61	498.7	0.2818	2995	365.7	1.78
R450A	39.4	25.09	200.1	0.5616	2665	228.8	1.25
R450A	39.7	24.72	200.1	0.5015	2481	217.3	1.232
R450A	39.9	25.66	200.1	0.409	2205	225.6	1.207
R450A	39.91	25.66	200.1	0.4287	2205	225.4	1.207
R450A	40.18	27.61	200.1	0.4381	2259	254.9	1.206
R450A	39.96	27.35	195.4	0.4014	2220	253.9	1.201
R450A	39.3	27.07	200.1	0.3974	2242	261.6	1.206
R450A	39.28	26.86	200.1	0.3761	2185	257.4	1.2
R450A	39.2	26.62	200.1	0.357	2127	253.5	1.197
R450A	39.95	27.16	200.1	0.3192	2065	249.1	1.199
R450A	39.62	30.14	200.1	0.693	3136	344.7	1.268
R450A	40.5	32.25	345.4	0.7664	5062	425.7	2.037

Ref	T_{sat} [°C]	T_{wall} [°C]	G [kg/m^{2}s]	x [-]	h [W/m^{2}K]	ω_h [W/m^{2}K]	ΔP [psi]
R450A	39.15	31.21	350.1	0.7255	4983	439.6	2.05
R450A	39.59	30.67	350.1	0.6156	4353	383.4	1.926
R450A	39.69	29.6	350.1	0.5143	3665	331.4	1.776
R450A	39.47	28.4	350.1	0.3854	3161	297.2	1.618
R450A	39.45	26.79	350.1	0.2492	2541	255.7	1.457
R450A	39.56	32.97	486	0.8152	7043	576.7	3.283
R450A	39.44	32.91	486	0.8221	7078	582.3	3.301
R450A	39.3	32.22	486	0.7333	6334	521.1	3.133
R450A	40.01	32.03	490.7	0.6218	5626	450.5	2.885
R450A	39.12	30.63	486	0.5283	4959	412.3	2.619
R450A	39.84	29.86	490.7	0.4199	4094	341	2.277
R450A	40.28	28.57	490.7	0.2828	3277	283.4	1.921